Studies of Sample Compartmentalization By Microfluidic Methods

Thomas Schneider

A dissertation
submitted in partial fulfillment of the
requirements for the degree of

Doctor of Philosophy

University of Washington
2012

Reading Committee:
Daniel T. Chiu, Chair
Frantisek Turecek
Bo Zhang

Program Authorized to Offer Degree:
Chemistry

University of Washington

Abstract

Studies of Sample Compartmentalization By Microfluidic Methods

Thomas Schneider

Chair of the Supervisory Committee:
Professor Daniel T. Chiu
Department of Chemistry

Miniaturization of reaction volumes into nanoliter sized droplets makes today's chemical analysis cheaper, faster, and more sensitive. These droplets can be generated by a variety of microfluidic methods that provide great control over size and composition, and can be performed at high speed. Other methods for droplet mixing and docking have been developed to allow droplet manipulation and subsequent analysis in continuous flow. These methods are designed to be modular systems, allowing the user to interchange or combine different methods in a "Lab on a Chip". The coupling of droplet generation, droplet manipulation, and analysis modules can be challenging if there is a mismatch between droplet generation frequency and time required to perform additional tasks in separate modules. As a result, droplet microfluidic methods can be very complex and can be less attractive for end-user applications, in particular in the biological sciences.

During the past years, a new generation of microfluidic droplet platforms emerged which is called self-digitization and is novel for its simplicity. In this method an aqueous sample is compartmentalized into smaller droplets by an immiscible phase and stored on-site. Self-digitization does not require complex microfluidic design or complex pumping and valving technologies to generate droplets. The volume of these droplets is predefined by the geometry of microfluidic wells and this gives rise to loss-less filling of large arrays of nanoliter wells. The droplets can then be addressed and monitored over time as their positions are registered in an array of static droplets.

This thesis summarizes the progress in the development of sample self-digitization in microfluidic arrays of side chambers and bottom wells, and provides a perspective view of the potential applications of this next generation droplet platform.

TABLE OF CONTENTS

LIST OF FIGURES

Figure Number Page

LIST OF TABLES

Table Number Page

LIST OF SYMBOLS

α	Contact angle
γ	Interfacial tension
δ	Inter-well spacing
δ_C	Distance before constriction
η, η_{CP}	Dynamic viscosity
μ	Kinematic viscosity
ρ	Density
A, A_{well}	Area, cross-sectional well area
Ca	Capillary Number
c, C	Concentration
d	Well/chamber depth
d_L	Laser induced displacement
E	Young's Modulus
f, f_{total}	Filling efficiency, total filling efficiency
h	Well/chamber height
H_m	Main channel height

k	Number of target particles
l	Well/chamber length
l_C	Constriction length
n	Number
o	Chamber overlap
p	Probability
R, R_{total}	Filling ratio or retention, total filling ratio or retention per chip
t, T	Time
u, u_{CP}	Linear flow velocity, linear flow velocity of continuous phase
V, V_w, V_{Drop}, $V_{Chamber}$	Volume, well volume, droplet volume, chamber volume
w	Well/chamber width
W	Well overhang
W_C	Constriction width
W_m	Main channel width

LIST OF ACRONYMS

BF	Brightfield
CFD	Computational Fluid Dynamics
CHF	Critical Heat Flux
CP	Continuous Phase
CTC	Circulating Tumor Cell
DP	Disperse Phase
dLAMP	digital Loop-mediated DNA Amplification
dPCR	droplet Polymerase Chain Reaction
ddPCR	digital droplet Polymerase Chain Reaction
ESI	Electro-Spray Ionization
F	Fluorescence
HTC	Heat Transfer Coefficient
ITO	Indium Tin Oxide
MS	Mass Spectrometry
PCR	Polymerase Chain Reaction
PDMS	Polydimethylsiloxane
SD	Self-Digitization

SLM	Spatial Light Modulator

ACKNOWLEDGEMENTS

I would like to express my sincere appreciation to the University of Washington, in particular to the Department of Chemistry and its current and past faculty members, especially Professor Daniel T. Chiu, Professor Frank Turecek, and Professor Bo Zhang. Additionally, I would like to thank my fellow graduate students and colleagues, my friends and family for their support.

CHAPTER 1

INTRODUCTION – A DROPLET PERSPECTIVE

1 Introduction

Today's chemical research is at a fast pace. Chemical analyses are expected to be accurate, cost-effective, fast, reliable, and sensitive. The shrinking of reaction volumes and the shrinking of sample handling into tiny microchannels that are often much smaller than a human hair met these expectations and was mainly driven by advances in microfabrication. The evolving small scale applications were often coined by the term microfluidics. Microfluidics can be defined as fluidic applications that are on the scale of micrometers or smaller and are based on microfabrication methods [1,2]. Microfluidics has been a thriving academic research field for over 20 years. During that time the field was driven by great expectations and challenges in everyday applications [3].

Out of the field of microfluidics emerged early on the field of droplet microfluidics. Droplet microfluidics takes advantage of the small scale and uses immiscible phases to create droplets as reaction and transport vehicles [4]. This field showed similar cycles of expectations and challenges as the field of microfluidics, although at an even faster pace. This chapter will give a brief summary of the field and it will provide a perspective of new directions for the field of droplet microfluidics. Other sub-fields emerged from microfluidics over the years including digital microfluidics, optofluidics, and paper microfluidics, among others. These fields of research are beyond the scope of this perspective and the interested reader is referred to the numerous well written reviews that cover these topics [5-11].

1.1 *Systems for Droplet Generation*

The central aspect of droplet microfluidics is the ability to form droplets of precise volume and composition. There are a variety of methods to generate droplets on microfluidic platforms. The majority of these methods can be classified as dynamic systems that rely on in-flow droplet generation. Among the dynamic systems is the plug generation at T-junctions [12] and the droplet generation by hydrodynamic flow focusing [13]. The fluids used in these systems are typically driven by syringe pumps, but other methods have been used to generate droplets in these systems including compressed air, vacuum, or centrifugal platforms [14]. The sample interaction and manipulation in these systems is conducted in continuous flow, which is very appealing to high throughput applications that have the potential to generate millions of monosized microdroplets per second (Figure 1a & b). The sample handling is often developed separately in modularized systems. These modules can perform a variety of tasks including droplet mixing [15], droplet splitting/fusion [16,17], or freezing of droplets [18]. Downstream coupling of droplet generation and droplet processing can directly impact the robustness of the system and can constrain the utility of the application. Furthermore, tracking and tracing of individual droplets over time which is of importance for time-dependent assays can be a challenge. For such assays the droplets tracking can be accomplished by labeling or incorporating the droplets with colored barcodes [19]. Such methods, however, add significantly to the complexity of the system.

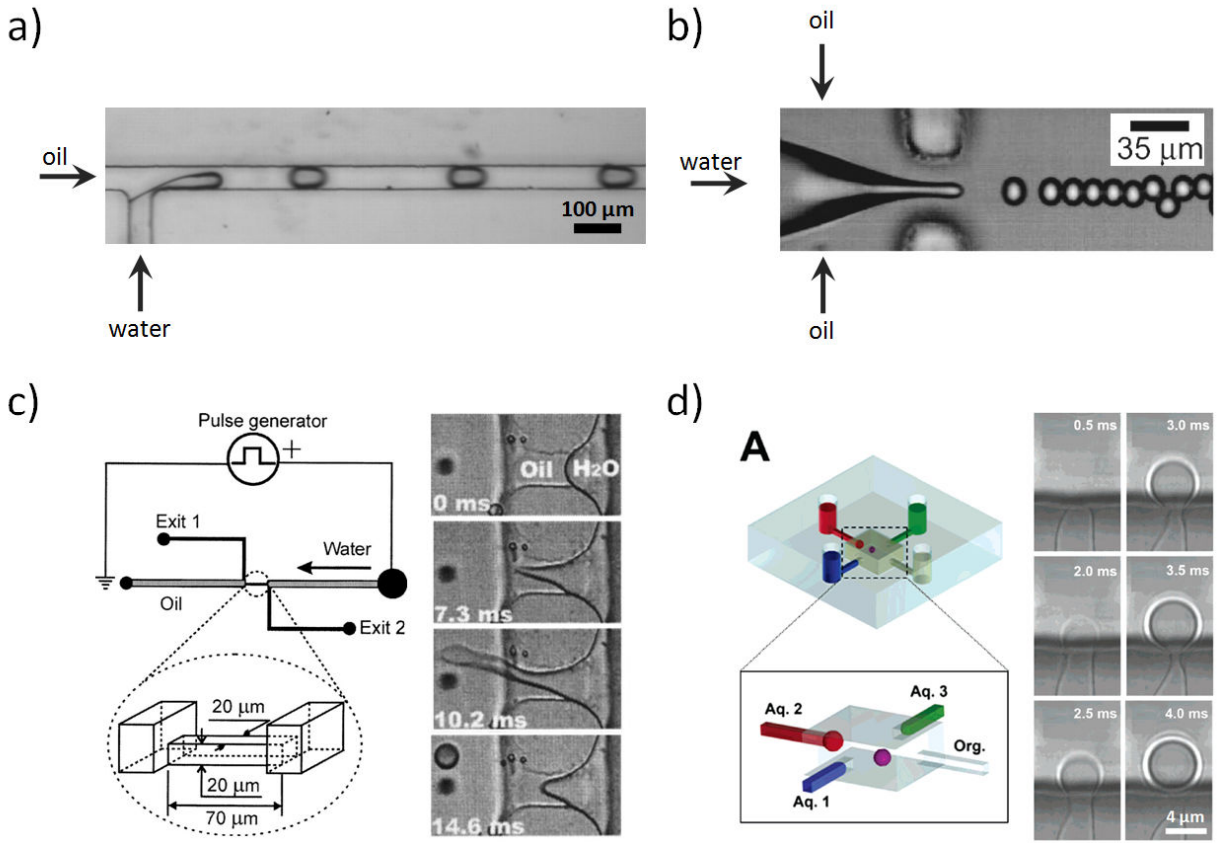

Figure 1. Dynamic droplet generation at a T-junction (a) and by Flow Focusing (b). Reprinted (adapted) with permission from [20]. Copyright (2006) American Institute of Physics. c) Droplet generation on demand based on electric fields (Reprinted (adapted) with permission from reference [21]. Copyright (2005) American Chemical Society) and d) based on pressure using micromanipulators (Reprinted (adapted)with permission from reference [22]. Copyright 2006, American Chemical Society).

The above methods are great for high-throughput applications. There are, however, other applications that do not require large sample throughput, but need greater control of the

downstream sample processing. Droplet on demand systems have been developed to address the need for slow sample processing (Figure 1c & d). These systems give precise control over droplet size and composition at very low throughput (often one droplet at a time) [21-25]. Droplet on demand systems have been specifically developed for processes that require seconds to minutes for completion (*e.g.*, nanosurgery on single cells [26,27]). A related but distinct field is digital microfluidics and has been thoroughly reviewed elsewhere [11].

1.2 *Systems for Droplet Docking and Storage*

Droplet microfluidics has been shown to be a simple, robust, and versatile method. Droplet processing downstream in modules directly coupled to the droplet generation has proven to be much more challenging. While methods for merging/splitting/mixing exist and have been successfully implemented, they have not shown the robustness necessary to achieve commercial viability. Robustness and flexibility in the downstream processing may not be an issue for some applications (*e.g.*, kinetics. synthesis) [18,28,29]. Other methods, however, require better control over droplets during the processing downstream. These methods include assays that require long term storage of droplets (*e.g.*, protein crystallization, cell culture). As a result, various "docking" strategies to store and handle droplets have been developed. Droplet docking applies physical means (*i.e.*, vertical posts, bypass traps, or side wells) in order to hold a droplet in place downstream while the droplet generation continuous up-stream. Different variations of docking systems have been conceived and may be classified in systems that require continuous flow for the droplets to remain docked and those systems that require no flow after droplet docking is completed. The former systems have been initially developed for perfusion based cell culture and

the study of enzyme kinetics [30,31]. These methods include bypass traps and vertical posts (Figure 2a & b). The concept was then rapidly applied to droplets [32-36] and allowed to combine the advantages of dynamic systems with stationary droplet analysis. The requirement of constant flow for the droplets to remain docked can be used as an advantage when the droplets are to be removed. After the droplets are docked and further analysis steps are completed, the flow can be interrupted or reversed which leads to the clearing of the droplets from the traps.

Other droplet docking systems were developed based on wells placed downstream at the side or at the top of a main channel carrying sample plugs. The sample plugs become docked when they pass by the wells which allows them to change to their least energy shape in the form of spherical droplets (Figure 2c & d) [37,38]. Another method used for docking droplets was presented with constricted channels that are shaped in the form of the droplets generated upstream [39]. The droplets flow through these constrictions. The droplets become immobilized and available for further analysis when the flow is stopped.

All of these docking methods were developed for specific applications and with a focus on keeping the droplets docked and separated from each other. These methods therefore required complex channel geometries. A simplified approach to docking that is less dependent on channel geometry was subsequently presented in the form of a large reservoir that takes advantage of high droplet density and the spherical shape of unconfined droplets to allow storage [40,41]. This method of droplet storage can be of great advantage for high throughput applications, but may be disadvantageous for applications that require sample separation to avoid cross-contamination or fusion between droplets.

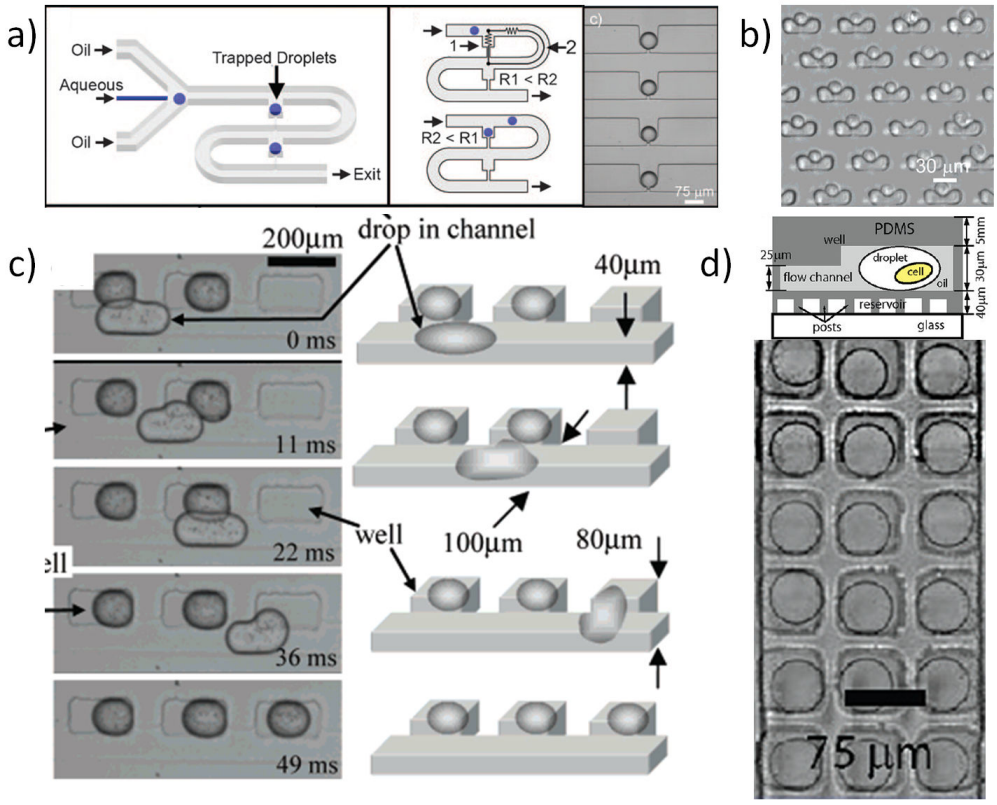

Figure 2. Systems for droplet docking and storage: a) in-flow docking systems with by-pass traps (Reprinted (adapted) with permission from reference [35]. Copyright (2009) Wiley-VCH Verlag GmbH & Co.) and b) docking by vertical posts (Reprinted (adapted) with permission from reference [30]. Copyright (2006) American Chemical Society), c) droplet storage in side wells (Reprinted (adapted) with permission from reference [37]. Copyright (2007) American Chemical Society) and d) top wells (Reprinted (adapted) with permission from reference [38]. Copyright (2009) American Chemical Society).

Overall the different droplet generation and docking/storage methods that have been developed fulfill specific needs and present applications with advantages and disadvantages. The use of applications based on droplet microfluidics, however, had limited success in industrial

applications despite the compelling methods, designs, and procedures that have been developed so far. The inherent challenges of combining individual modules of droplet microfluidic applications are reflected in the most successful use of droplet microfluidics in commercial applications: droplet based polymerase chain reaction (PCR). The system originally developed by QuantaLife and now marketed by BioRad Inc. employs the dynamic droplet generation by flow focusing at first. However, the droplets are subsequently collected off-chip in Eppendorf tubes for further processing. The droplets are then thermo-cycled and finally transferred back into a chip cytometer for data acquisition and analysis.

1.3 *Next Generation Droplet Platforms*

A new generation of droplet microfluidics has started to be established in recent years. Where current systems preform droplets and then deposit them elsewhere for processing, these new systems form the droplets on-site and the droplet size is determined by the storage chamber geometry. This provides much greater tunability over droplet volumes, and simplifies the equipment needs to generate droplets. These systems are also significantly different from other systems that take advantage of surface wetting by the aqueous phase to trap small sample volumes in chambers [42,43]. These new generation devices are preferentially wetted by the oil phase, thus maintaining many of the favorable properties of droplet based systems such as interfacial control, while utilizing some of the favorable features of geometry induced digitization.

Two new generation systems include the SlipChip (Figure 3a,b) [44,45], and the Self Digitization (SD) Chip (Figure 3c,d) [46,47]. While they share many features in common the

actual mechanisms of droplet formation/digitization are unique. The SlipChip consists of two separate plates, each containing a pattern of wells and ducts. The plates are aligned under oil, which eliminates air bubbles, prewets the device surface, and serves as a lubricating layer for facilitating controlled slipping of the plates relative to each other. In one alignment there is a fluidic path that allows the aqueous solution to enter (under simple air pressure/actuation) and fill the main fluidic path while oil drains out between the two plates. The device is then slipped to a new alignment that isolates the wells creating digitized droplets (Figure 3a). One unique feature of this system is the ability to perform multistep processes.

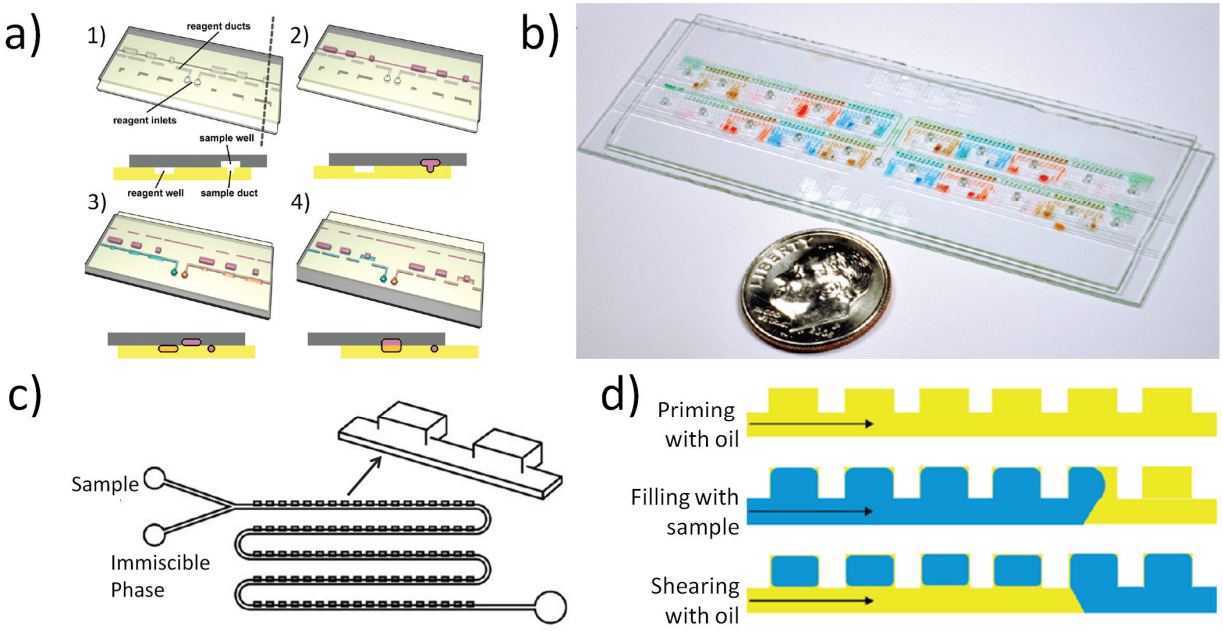

Figure 3. Next generation droplet platforms: a, b) Slip Chip (Reprinted (adapted) with permission from reference [45]. Copyrights (2010) American Chemical Society) and c, d) SD Chip (Reprinted (adapted) with permission from references [46]. Copyrights (2010) American Chemical Society).

The SD Chip consists of an array of chambers/wells connected by a continuous channel network. The entire device is prefilled with oil and the aqueous solution is loaded using simple air pressure/actuation. The geometry of the device and interfacial properties of the aqueous solution spontaneously drives the aqueous solution into the side chambers. After the aqueous solution is loaded more oil follows to isolate the wells from each other, thus digitizing the droplets (Figure 3d). This system does not require moving parts, is capable of achieving very high well density, and allows lossless filling of the aqueous sample.

1.4 *Biological Applications*

Droplet microfluidics is increasingly becoming an enabling technology for other applications. Most prominent and most successful in terms of commercialization is the use of droplet microfluidics for Digital PCR [48,49]. Droplet digital PCR (ddPCR) is currently marketed by BioRAD Inc. (Figure 4) and RainDance Technology. Both systems use dynamic droplet generation to emulsify the sample and conduct PCR cycling off-chip. The final analysis is then conducted in a microfluidic channel. Commercial ddPCR systems find growing acceptance in the research community and provide a powerful tool for high-throughput studies on biomarkers [50,51]. A similar approach, although not commercialized yet, is a microfabricated emulsion generator array (MEGA) chip [52] which uses pneumatic systems to create nanoliter droplets. Similarly to the already commercial systems, droplets generated by the MEGA system are cycled off-chip and subsequently analyzed in a conventional flow cytometer.

In contrast to that are the next generation droplet platforms, the SlipChip and the SD Chip. Currently the main application in these systems is droplet based digital PCR. In contrast to

the methods mentioned before, these systems allow droplet generation, cycling, and analysis on the same chip without the need for sample transfer or complex valving systems. The data read-out can subsequently be conducted by conventional plate readers. This capability and the simplicity of droplet generation may be advantageous for end-user applications. These systems have been recently shown to be a versatile and powerful tool for multiplex PCR [53,54] and digital loop-mediated DNA amplification (dLAMP) [47,55].

Growing interest is also in the use of droplet microfluidics as a pre-sampling tool for molecular analyses and molecular screening by (electrospray) mass spectrometry [56-60]. Current analysis of individual cells by Matrix-Assisted Laser Desorption/Ionization (MALDI) [61-63] may eventually be realized for individual cells processed by droplet microfluidics and coupled directly to mass spectrometry. The potential of droplet microfluidics as a powerful tool for single cell studies has been demonstrated since the emergence of the field. Recent studies show a potential commercial direction with single cell screening assays [64,65]. Such assays have generated interest for droplet microfluidics as a potential application for the production of monoclonal antibodies from individual hybridoma cell clones [66].

Other applications of droplet microfluidics include the study of crystal growth [37,46,67] and enzyme kinetics [38,68], as well as studies on directed evolution by *in vitro* selection [69], and applications for small molecule synthesis in microdroplets [70] and for pharmaceutical applications [71,72]. Droplet microfluidics showed its broad applicability in various fields of research. More applications have been presented and are beyond the scope of this perspective. The interested reader is referred to comprehensive reviews on droplet microfluidics [73-76].

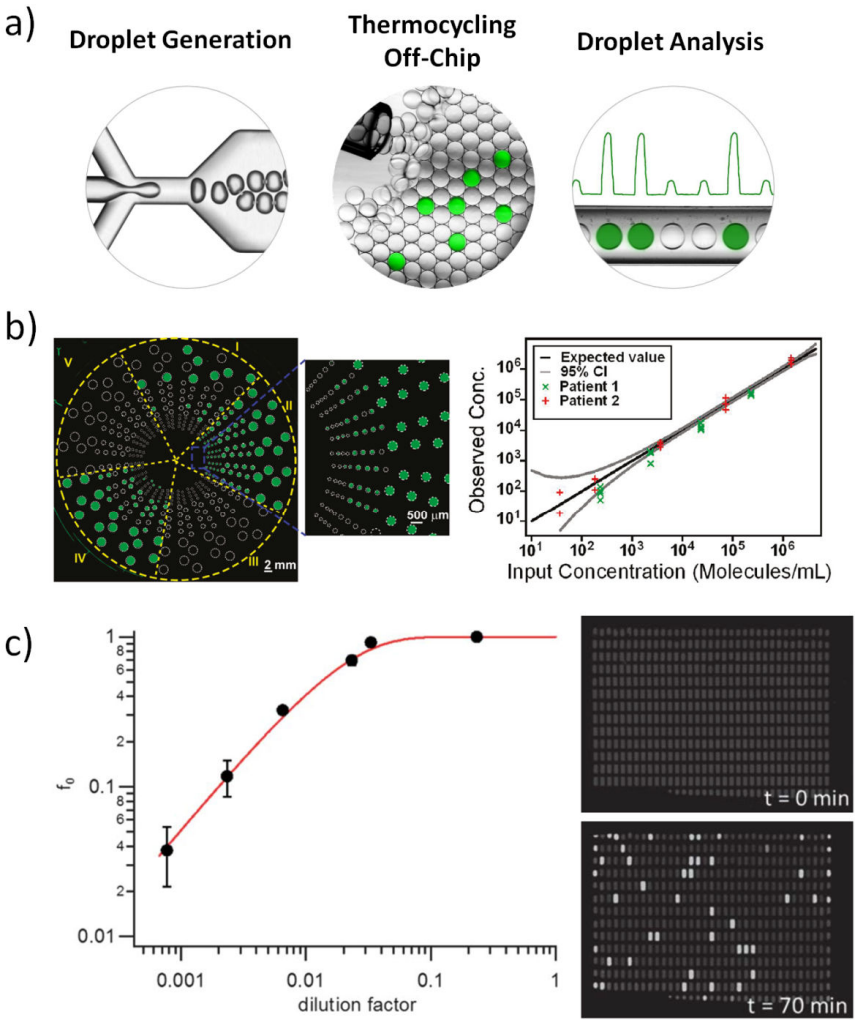

Figure 4. Biological Applications of dPCR. a) ddPCR in a commercial format available from BioRAD. b) Multiplex dPCR with a large dynamic range in a SlipChip (Reprinted (adapted) with permission from reference [54]. Copyright (2011) American Chemical Society) and c) digital loop-mediated DNA amplification (dLAMP) in a SD Chip (Adapted with permission from reference [47]. Copyright 2012).

CHAPTER 2

SAMPLE SELF – DIGITIZATION IN MICROFLUIDIC BOTTOM WELLS

2 Sample Self – Digitization in Microfluidic Bottom Wells

2.1 *Introduction*

Droplet microfluidics was shown in the previous chapter as a very attractive technology for the handling and manipulation of small sample volumes. Different methods were summarized that allow droplet generation in dynamic and on-demand systems [13,20-23,25,77]. These methods were developed as individual modules and they were shown to have many advantages (*e.g.*, high droplet generation frequency, control over droplet size). These systems also presented challenges, particularly when individual modules were combined, which can result in mismatches between droplet generation and droplet handling downstream. As a result, additional methods were developed that allow docking and storage of droplets [32-36]. The next generation droplet microfluidic platforms were introduced and shown to take a different approach by generating and storing droplets on-site, without the need for modular systems.

Two types of next generation droplet microfluidic platforms have been developed so far: the SlipChip (Ismagilov group at CalTech) and the Self-Digitization Chip (Chiu group at UW). These next generation droplet microfluidic platforms have the following features: *i*) they allow droplet generation, storage, and manipulation in microfabricated wells on the same chip, *ii*) the droplet size is determined by the geometry of the well, *iii*) the chip requires no complicated valving and pumping, and *iv*) the method has the potential for loss-less sample digitization. In a simplified way these droplet microfluidic methods can be described as a miniaturization of the microwell plate, a standard tool for today's diagnostics. However, unlike in microwell plates, there is no pipetting required to aliquot a sample into the wells of the next generation platforms and the wells are ten- to one hundred times smaller (nL vs. tens of μL).

Recently a novel self-compartmentalization method was presented that has all of the features for the next generation droplet microfluidic platform and is called the Self-Digitization (SD) Chip [46]. This method was shown to compartmentalize an aqueous disperse phase (*DP)* sample plug by a continuous oil phase (*CP*) at low capillary numbers (*Ca)*; the capillary number is a dimensionless number used to characterize viscous and interfacial forces in multiphase flow systems and can be defined as $Ca = \mu u/\gamma$, where μ is the *CP*'s viscosity, u is the linear flow velocity, and γ is the interfacial tension. In this chapter the SD Chip and the characterization of the method will be presented. Subsequent studies to optimize and improve sample compartmentalization will be presented and discussed.

2.2 *Results and Discussion*

2.2.1 Sample Self-Digitization in an Array of Side Chambers

The filling and self-digitization of an aqueous sample was investigated in initial studies with a single serpentine microfluidic channel (Figure 5). The main channel had dimensions (width, height: W_m, H_m) smaller than the side chambers (width, height, length: w, h, l) positioned adjacent to the channel. Two immiscible phases, a continuous oil phase (*CP*) and an aqueous disperse phase (*DP*), were introduced into the chip by two inlets and driven manually by a micromanipulator (Figure 5). Studies with the single channel side chambers included a parametric study with two main design variations (*i.e.*, a square side chamber and a side chamber with drainage channels). Preliminary studies investigated the filling in variations of the side chamber dimensions and indicated a potential application for separation of concomitant polymorphs [46].

In order to better understand the filling mechanism in the side chamber chips, a computational analysis was conducted with computational fluid dynamics software (Ansys Fluent). This computational analysis was used to investigate different parameters that may impact the filling. Among the parameters tested was the dynamic viscosity of the continuous phase (η_{CP}), changes in the interfacial tension (γ), the hydrophobicity of the microfluidic chip represented by the contact angle (α), the linear flow velocity of the *CP* (u_{CP}), as well as the dimensions of the side chamber (w, h, l). Transient multiphase simulations were conducted for the different parameters and the volume of the *DP* retained in the side chamber was directly read out from Fluent and normalized to the side chamber volume ($V_{Drop}/V_{Chamber}$).The use of transient

multiphase simulations allowed the visualization of the different stages in the self-digitization for different parameters: 1) Priming with *CP*, 2) Filling with *DP*, and 3) *DP* shear off by the *CP* and retention of the *DP* in the side chamber (Figure 5c).

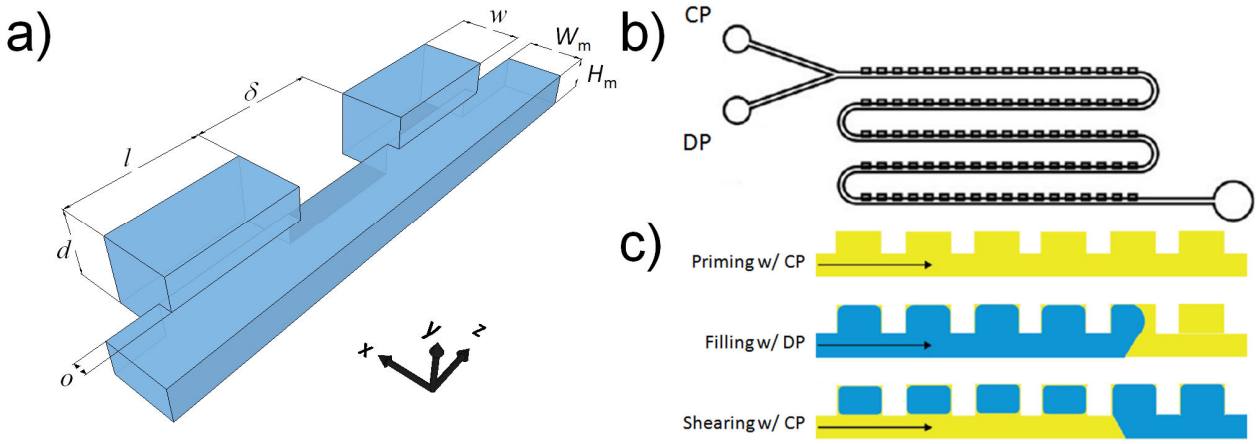

Figure 5. Side chamber SD chip: a) Conceptual side chamber design with dimensions length (l), width (w), and depth (d). The side chamber is connected to a main channel of height (H_m), width (W_m), and with an overhang (o). b) Chip used in the studies with two inlets for CP and DP supplied manually by a micromanipulator. c) Scheme of loss-less digitization in side chamber chip by first priming with CP, followed by filling with DP and shearing off the DP by the CP. (Reprinted (adapted) with permission from references [46]. Copyrights (2010) American Chemical Society).

An example of a 3-dimensional channel simulated with Fluent shows the sequences of these stages (Figure 6). In this example a single side chamber ($w \times h \times l$ = 100 µm × 50 µm × 50 µm) was attached to a main channel (W_m = 50 µm, H_m = 25 µm) and is shown in a top view. An aqueous sample plug (red in Figure 6) was simulated to flow in the main channel. The main channel was prefilled with oil (blue in Figure 6). Twenty five milliseconds after starting the flow,

the *DP* fills into the side chamber (Figure 6b). Once the side chamber is filled, the remaining *DP* is pushed out through the main channel by the *CP* (t = 75 ms, Figure 6c). Subsequently, the *DP* is sheared off by the *CP* and a *DP* droplet is retained in the side chamber (t = 200 ms, Figure 6d).

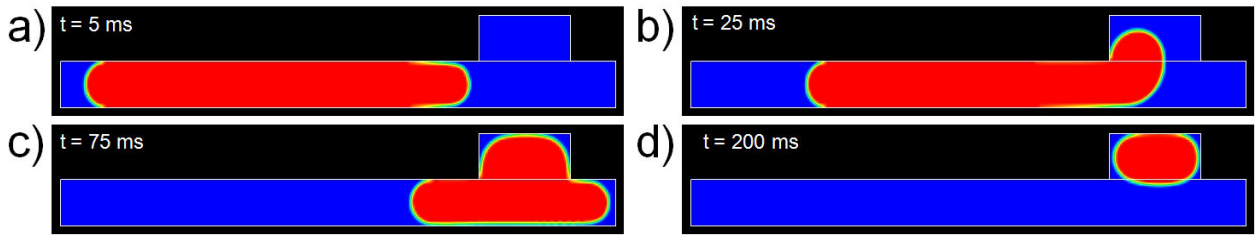

Figure 6. Example sequence of droplet breakup from a plug of water in light mineral oil (μ = 30.0 cSt) simulated with Ansys Fluent at u_{CP} = 5.0 mm s^{-1}, γ = 40.0 mN m^{-1}.

The results of the simulations with a single side chamber showed that there is a strong trend in droplet retention for different parameters. Parameters such as linear flow velocity of the *CP* (u_{CP}) during the shearing phase, interfacial tension (γ), as well as the contact angle (α) all affected the way the *DP* was retained in the side chamber (within the accuracy of the individual simulations). By combining the results from different simulated parameters (*i.e.*, η_{CP}, γ, u_{CP}) and collapsing the data sets for each contact angle, it can be seen that the droplet retention is successful below a $Ca \sim 0.01$ with minor dependence on the contact angle (for $\alpha > 120°$; Figure 7). It has to be noted that surfaces exhibiting contact angles greater than 90° are regarded as hydrophobic and typical contact angles for untreated PDMS are 100° – 110° [78,79]. Larger contact angles can be achieved by nano- and micropatterning the PDMS surface and were shown to exceed 160° [79]. The simulations shown here are idealized cases, where the surface is perfectly flat. The contact angles were therefore chosen higher than those reported in literature.

Contact angle measurements on flat PDMS surfaces resulted in similar results than those reported in literature (*i.e.*, 95-110°). However, the measurement of contact angles in small confined cavities of the side chamber channels proved to be challenging and was not successful.

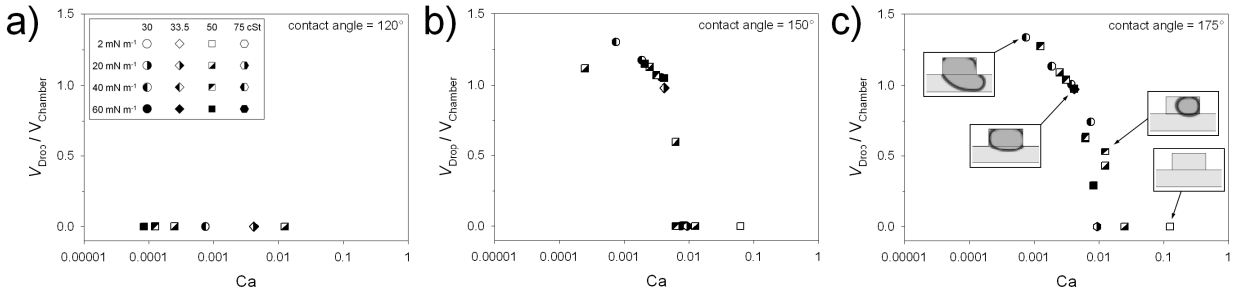

Figure 7. Effect of capillary number on the normalized droplet volume fraction ($V_{Drop}/V_{Chamber}$) retained in the chamber for different contact angles: a) 120°, b) 150°, and c) 175°. The contact angle is the angle between the tangent to the interface at the wall as measured inside the secondary phase (water) and the wall itself. Note the effect of contact angle on droplet retention, wherein the surface needs to be sufficiently hydrophobic ($\alpha >> 90°$) in order to allow flow into and to keep the droplet inside the chamber. Also note the abrupt decrease in droplet volume fraction above a critical capillary number for large contact angles. Reprinted (adapted) with permission from references [46]. Copyrights (2010) American Chemical Society.

2.2.2 Strategies to Make Self-Digitization Larger and Faster

Following the initial success with the side chamber SD Chips we embarked on a journey to explore possibilities to allow for a faster filling of larger chips. The filling strategy used in our side chamber study [46], although successful, had several limitations in terms of overall through-put. The use of micromanipulators for the filling had an inherent user bias and was limited to small chips (10-100 side chambers) to allow filling and sample digitization in a reasonable time (*i.e.*, minutes). Additionally, the use of side chambers with a small opening to the main channel may hinder the addressability and accessibility of the digitized sample and its potential removal by external means (*e.g.*, lasers, micro-manipulators), as the droplet is confined by 6 chamber walls.

As a result several strategies motivated the future work and are outlined as follows:

1) Expand the self-digitization from side chambers to bottom wells, which may reduce the overall foot print and improve sample addressability.

2) Increase the number of digitized samples by increasing the number of side chambers and wells from 10's to 1000's to improve statistics.

3) Expand the filling scheme from a single main channel to multi-bifurcated channels which will allow digitization of 100s of well in parallel and reduce overall processing time

4) Modify the filling strategies from manual filling by micromanipulators to an automated filling system (*e.g.*, pumps, pressurized air).

5) Develop a image analysis software to process large image sets of thousands of wells to allow unbiased data quantification

2.2.3 Sample Digitization in Bottom Well Chips

In the first step, a bottom well SD Chip was designed that consists of a flat main channel placed on top of a bottom well (Figure 8). The serpentine channel used in the side chamber study was replaced by multiple well channels placed next to each other and connected through bifurcations, in order to allow higher sample throughput in shorter time. As a result, the bottom well SD Chip design has two main features that differ from the side chamber SD Chip design. First, the bottom wells are designed to be underneath the main channel. This has the advantage of creating denser arrays of wells. It also may be advantageous to applications requiring heating of compartmentalized droplets (*e.g.*, PCR) by providing an evaporation barrier via the oil filled main channel on top of the well. The second difference to the side chamber SD Chips stems from the connection of the well to the main channel. Unlike the side chamber SD Chip, where the main channel connection is only through a narrow slit, the bottom well connection to the main channel is much larger and includes the entire cross section of the well (red area in Figure 8b). The open wells in the bottom well SD Chips may be advantageous for applications requiring access to the droplet or components of the droplet by external methods (*e.g.*, optical tweezers, micropipettes).

The sample digitization was first investigated in arrays of squared bottom wells and with straight main channels. Subsequent optimizations included the addition of constrictions in the main channels, modifications to the outlet bifurcations of the main channels, and changes to bottom well geometry. The sample digitization was investigated in experimental studies by brightfield and fluorescence microscopy and by computational analysis using CFD (Figure 9).

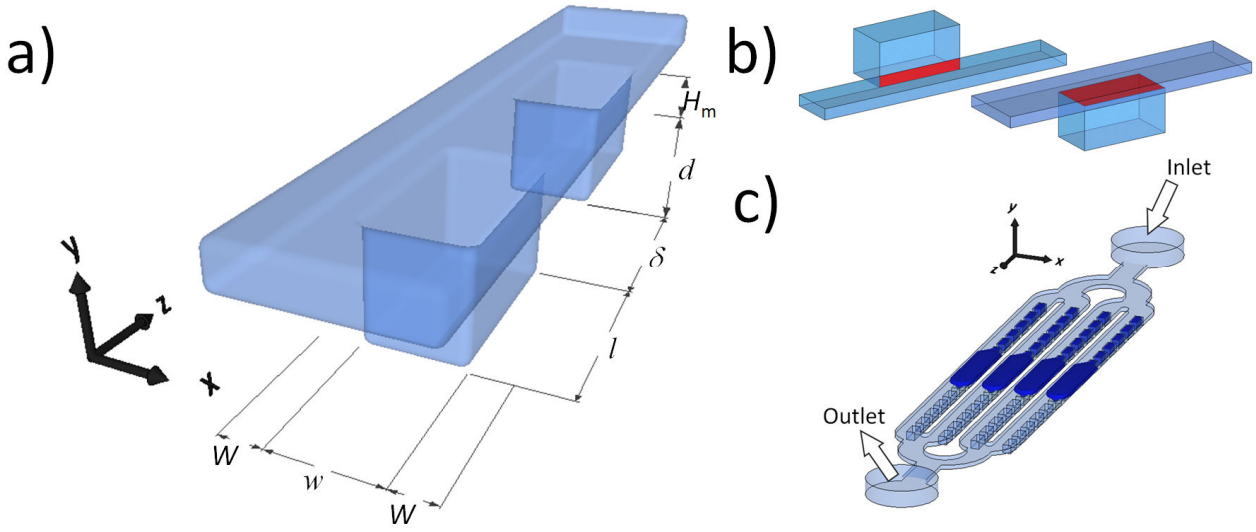

Figure 8. Bottom well SD Chip: a) Conceptual design of the bottom well chips with dimensions length (l), width (w), and depth (d). The bottom well is connected to a main channel of height (H_m) and width (W_m = w + 2W, wherein W is the overhang of the main channel measured perpendicular to the flow direction (z – direction)). b) Difference in connection (red area) of chamber/well to the main channel in side chamber and bottom well chips. c) Scheme of loss-less digitization in a bottom-well SD chip with four parallel rows of 15 bottom wells per row that are connected by a main channel.

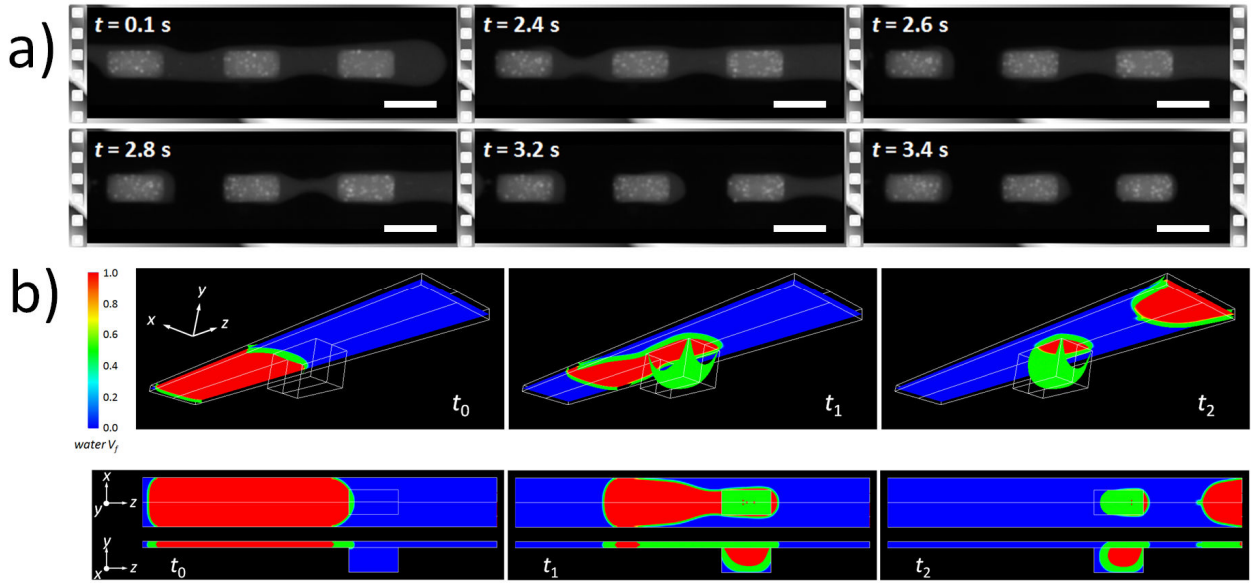

Figure 9. Sample digitization shown by fluorescence microscopy and CFD. a) Fluorescent image sequence of sample digitization in a 1,024 well chip at Ca = 0.015. Shown is the shearing of an aqueous DP sample (supplemented with 100 µM Fluorescein) by 50 cSt silicone oil with 0.01% w/w Gransurf 77 in three bottom wells imaged at the x-z-midplane. Note the nicking of the aqueous phase between wells before compartmentalization from the bulk DP. Scale bar corresponds to 200 µm. b) Example of well filling by 3-dimensional water-in-oil multiphase flow CFD analysis before (t_0), during (t_1), and after droplet breakup (t_2); shown are the color contours at the x-z- and y-z-midplane of the water volume fraction ranging from blue = oil to red = water and the water/oil-interface shown as an iso-surface (green). The flow in a) and b) is from left to right.

2.2.4 Sample Retention and Total Compartmentalization Efficiency

The compartmentalization of sample volumes in bottom well chips with straight main channels showed a strong dependence on the main channel's dimensions and viscous/interfacial properties (*Ca*). We conducted an extensive study with arrays of 1,024 wells per chip to investigate different parameters that affect the filling. These parameters included the main channel's overhang with respect to the well width (W/w), the normalized spacing between wells (δ/w), and the aspect ratio of the well with respect to the flow direction (l/w). The results from the parameter study are based on fluorescence microscopy images of filled wells (bright) with respect to the oil filled, non-fluorescent chip (black; Figure 9a). The results are presented as the retention ratio (R) and the total filling efficiency (f_{total}). The retention ratio is defined by the number of wells filled per chip, independent of wells that remain interconnected through the main channel. The filling efficiency is defined as the ratio of individually compartmentalized (not interconnected) sample volumes and is normalized to the cross-sectional area of a well.

Our study shows that the sample compartmentalization is dominated by viscous and interfacial forces, as represented by *Ca*. Our results also indicate a dependence of sample compartmentalization on channel geometry (W_m, H_m). Almost 100% of the sample can be retained in the wells at low *Ca* and over the entire range of channel overhang (W) studied (average R_{total} of 87.9 ± 4.3%, n = 7). The highest R_{total} of 98.4% was achieved in a chips with W/w of 0.25 and at *Ca* of 0.010 (Figure 10a). The compartmentalization of individual sample volumes (f_{total}), however, depends highly on interplay between W/w and *Ca* (Figure 10a). High f_{total} of up to 99.5 ± 0.5% (n = 2) were achieved at *Ca* of 0.030 and W/w of 0. However, some of the wells contained droplets that were much smaller than the wells. In straight channels without

overhang (W/w = 0) the overall trend in f_{total} and the number of smaller droplets per well is increasing with increasing *Ca* (Figure 10a). Droplets that filled out the entire cross-sectional area of the well were found at $W > 0$ and at *Ca* of 0.010 and 0.020. An average f_{total} of 74.2 ± 3.8% and 75.2 ± 6.2% was achieved for W/w = 0.25 (*Ca* = 0.010) and W/w = 0.50 (*Ca* = 0.020), respectively. This indicates a dependence of f_{total} on the overhang W and the *Ca* used during sample compartmentalization. The overall trend of W/w in terms of f_{total} is decreasing with increasing *Ca*.

Computational fluid dynamics simulations showed that no sample is retained when W was 0 (see Figure 12b). The simulations also indicated that a small W is required to allow for samples to be compartmentalized and retained. On-chip experiments with W/w of 0, however, showed sample retention (Figure 10a). These results could be explained by imperfections in the multi-layer microfabrication process. Minor misalignments in the fabrication process between the first layer (main channel) and the second layer containing the bottom well can result in edges that support droplet retention (~1-2 μm, measured by brightfield microscopy). In contrast, a larger W reverses the effect of high f_{total} and can be explained by the way the bulk *DP* is compartmentalized in each well (see Figure 9). The *DP* compartment in each well is pinched off from the bulk *DP* by the shearing of the *CP* between adjacent wells. Wider main channels result in weaker shear forces and allow adjacent wells to remain interconnected through a *DP* bridge in the main channel.

Based on the results from the overhang study (W/w), it could be argued that a higher inter-well spacing, δ, would be beneficial for higher f_{total} and R_{total}. We investigated δ normalized to the well width for W/w of 0.5. Our results show that when δ/w increases from 0.5 to 1.0, f_{total}

and R_{total} increase as well for *Ca* of 0.004 to 0.020 (Figure 10b). At higher *Ca*, however, both f_{total} and R_{total} approach zero (*i.e.*, 2.3 ± 0.6% and 3.6 ± 1.9%, respectively). At larger δ/w (2.0) the sample compartmentalization and retention decreases across all *Ca* studied. These results indicate that δ has similar effects on the breakup of individual droplets from the bulk *DP* as the main channel overhang (*i.e.*, by nicking or pinching during shearing by the *CP*). Furthermore, the inter-well spacing has a strong impact on the density of a bottom well array. Larger inter-well spacing reduces the overall sample volume that can be compartmentalized or retained in a chip for a given chip area *A*.

In some applications it is desirable to fill the entire chip with sample regardless of how the sample is digitized (max. R_{total}; *e.g.*, loss-less compartmentalization of small volumes that contain rare species). In contrast, other applications require individually compartmentalized samples that are digitized and separated from one another by the *CP* (*e.g.*, digital PCR [53,55]). In our study with straight main channels, we found that the optimal design for both high R_{total} and f_{total} (*i.e.*, 83.0 ± 5.0% and 84.5 ± 5.3%, respectively) was achieved for bottom well chips with a W/w of 0 and *Ca* of 0.02.

Another parameter with effects on sample retention is the well length, *l*, and the direction to the main channel flow. For W/w of 0.5 it was found that l/w of 0.5 (*i.e.*, a wide well perpendicular to the flow direction) is least beneficial for high f_{total} and R_{total}. Wells with a square cross section (l/w of 1.0) showed higher f_{total} and R_{total} with increasing *Ca*. The overall trend in sample compartmentalization and retention suggests a rectangular well placed in the flow direction (l/w) is most beneficial for high f_{total} and R_{total}. The highest values for f_{total} and R_{total} were

found in our study for *l*/*w* of 2.0 for *Ca* of 0.020 (f_{total} = 75.2 ± 6.2%) and for *Ca* 0.004 (R_{total} = 91.6 ± 4.4%), respectively (Figure 10c).

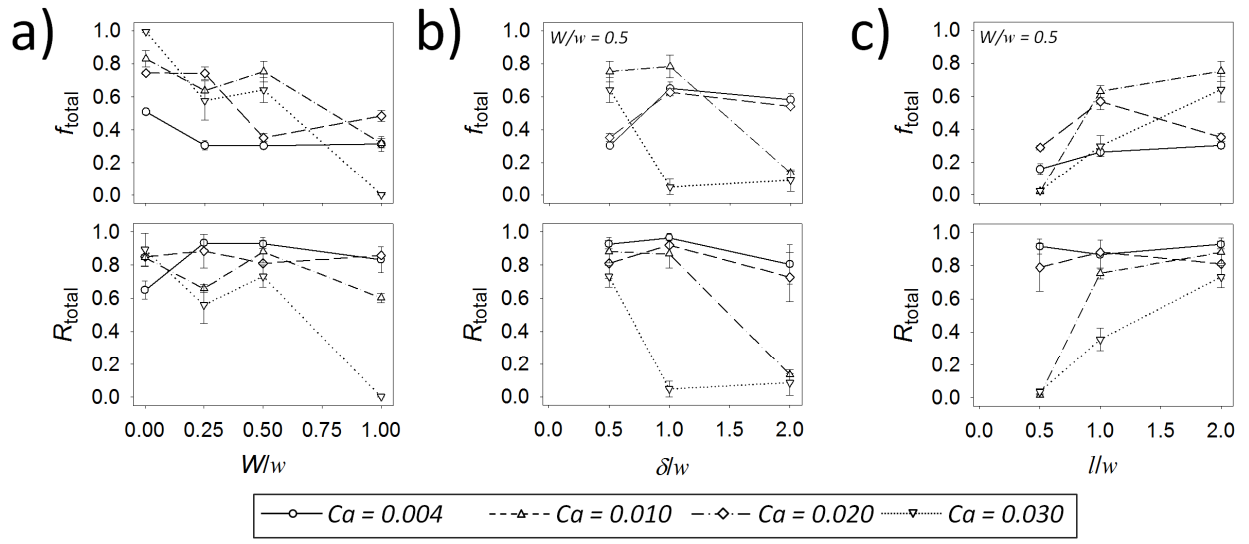

Figure 10. Results summary of parameters effecting the filling efficiency, f_{total}, and sample retention ratio, R_{total}, in bottom well chips with 20 µm tall (H_m) main channels. The graphs show the effect of a) the normalized main channel overhang, W/w, b) the normalized inter-well spacing, δ/w, and c) the well aspect ratio, l/w, with respect to the flow direction. Note that f_{total} accounts for individually compartmentalized sample volumes, while R_{total} is defined by the number of wells filled per chip. Data is shown as mean ± SD (n = 2).

There are, however, other parameters aside from f_{total} and R_{total} that can be quantified from the data. Bottom well chips with high R_{total} but lower f_{total} can be of interest to applications that require unequal sample sizes compartmentalized on a single chip. A typical example of a 1,024 well chip with high f_{total} and R_{total} is shown in Figure 11a. It can be seen that some of the wells are present in doublets, triplets, and higher numbers of interconnected wells. A histogram showing

the number of interconnected wells in this chip (Figure 11b) indicates that the majority of the individual samples are confined to single wells. The droplets in these single wells comprise a normalized area (A/A_w) of 0 – 0.75 (f = 2.3%) and 0.75 – 1.50 (f = 63.7%). Doublet wells, *i.e.* samples retained in adjacent wells and connected by a *DP* thread through the main channel (A/A_w of 1.5 – 2.5), made up 5.2% of f_{total}. Samples interconnected and retained in three or more wells were 6.8% of f_{total} in the example shown in Figure 11. The overall trend for the parameters tested in our study showed a decrease in the fraction of doublets and triplets and an increase in samples compartmentalized in single wells with increasing *Ca*.

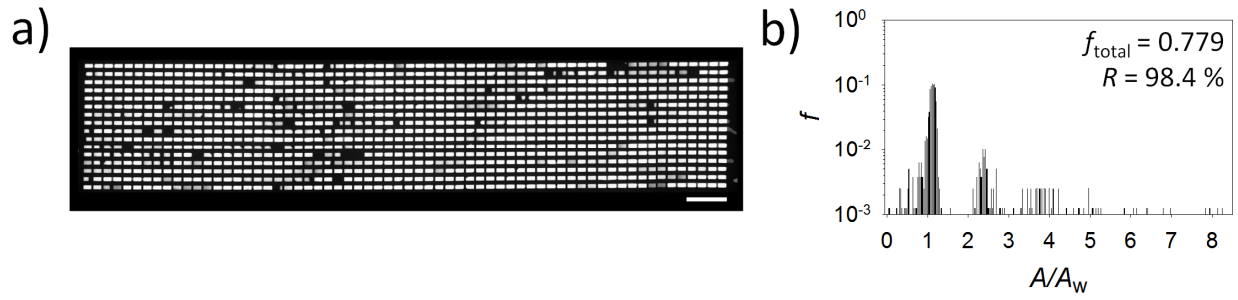

Figure 11. Example of improved sample compartmentalization in constricted bottom well SD chips: a) Fluorescent microscopy image samples compartmentalized in a chip with 1,024 bottom wells at Ca of 0.010 ($w = d = 100$ µm, $l = 200$ µm, $W_m = 25$ µm, $\delta = 50$ µm, $H_m = 20$ µm). The size bar corresponds to 1 mm. The filling efficiency, f, of the chip is shown in b), normalized by the ration of sample cross-sectional area, A, to the well area, A_w. Note that some of the samples comprise 2-8 wells and thus reduce f_{total} when compared to R_{total}.

In order to highlight the importance of *Ca* on the sample retention we combined the entire data from the parametric study into a single plot (see Figure 12a in next section). It can be

seen that there is a distinct trend in the retention of sample (R_{total}) with increasing *Ca*. Almost 100% of the sample can be retained in the chip at *Ca* below 0.020. At higher *Ca* the majority of the *DP* sample is flushed out of the chip by the shearing *CP*, thus decreasing R_{total}.

2.2.5 Computational Fluid Dynamics of Sample Compartmentalization

Computational fluid dynamics (CFD) was shown as a powerful tool to study process parameters for our side chamber SD Chips [46]. A similar approach was used to investigate parameters that can optimize the sample digitization in bottom well SD Chips.

Preliminary bench-top studies with bottom well chips and varying heights of the main channel (H_m) indicated a critical height above which the sample digitization is greatly reduced. In these studies, bottom well chips with well volumes of 2 nL were used. These chips had a normalized channel overhang (W/w) of 0.25, a normalized well spacing (δ/w) of 0.5, and a well aspect ratio (l/w) of 2.0. The experimental studies indicated that R_{total} and f_{total} approached zero when H_m was greater than 30-40 μm. To further investigate the effects of main channel geometry and changes in *Ca* on the sample compartmentalization we used CFD models of a single bottom well. The material properties (oil and water) used in on-chip experiments, were also used in the CFD studies. Unlike the on-chip studies, the CFD study allowed for the direct read-out of the retained *DP* sample volume and is presented in the *Ca* plot normalized to the well volume, V_w (Figure 12b).

In the studies with a main channel height of 25 μm (open symbols in Figure 12b) it can be seen that the V/V_w decreases with increasing *Ca* and approaches zero at *Ca* 0.020 (except for

studies with *W/w* = 0). Furthermore, with increasing *W/w* the ratio of retained sample volume increases as well. When *W/w* was 0 the sample was only retained at low *Ca*. This result indicates the requirement of a small main channel overhang to allow sample to be retained in the well. The overall trend of sample retention is similar between the on-chip and CFD data shown in Figure 12 when the *Ca* is used as an indicator for retention or no retention. The change in volume of the retained droplet can only be quantified by the CFD data. It must be noted that the retention data shown in Figure 12a is based on the samples' cross-sectional area, while in Figure 12b the sample volume is taken into account.

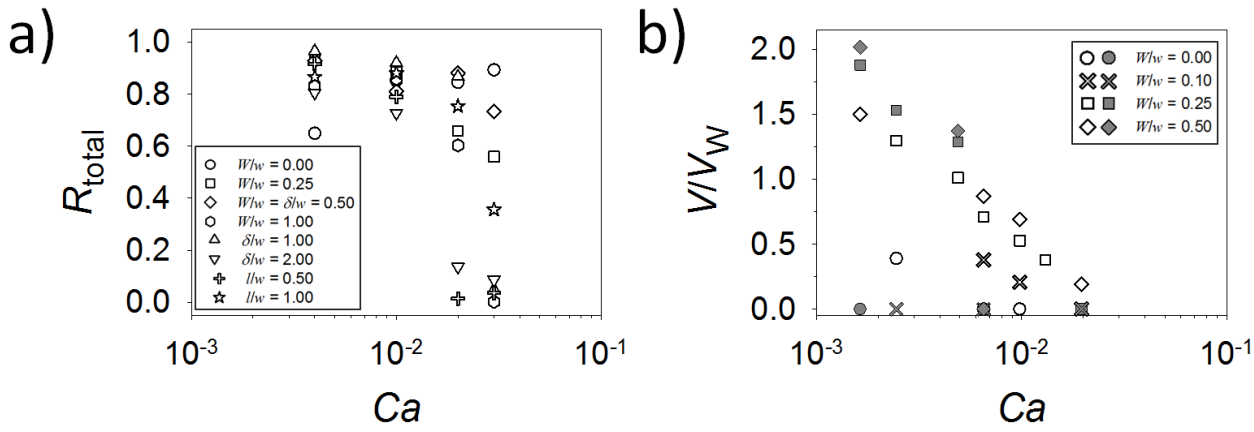

Figure 12. Trend of sample retention in bottom wells with respect to Ca. a) Combined results from the parametric study in chips with 1,024 wells based on R_{total}. Note the distinct cut-off in sample retention above Ca > 0.02. b) Results from a parametric CFD study with different H_m (white symbols = 25 µm, grey symbols = 50 µm). Note the similarity in retention cut-off (Ca) between a) and b) despite the difference in data used (area vs. volume of retained sample; see main text).

When H_m increased to 50 μm (grey symbols in Figure 12b) it was found that a larger fraction of the compartmentalized sample expanded into the main channel (therefore $V/V_w >> 1.0$), and the sample retention approached zero abruptly at a much lower *Ca* (0.0065) when compared to H_m of 25 μm (retention below *Ca* of 0.020). However, at $W/w < 0.25$ none of the *DP* sample is retained in the well when *H* was 50 μm and for the *Ca* range used in the CFD study (*Ca* = 0.0016 – 0.0196).

The results from the CFD study for variations in main channel height, H_m, indicate that the sample retention and compartmentalization are not only dependent on the main channel's overhang (*W*), but are also greatly affected by *H*. This observation indicates that the pinching of the *DP* by the shearing *CP* is dominated by the main channel geometry (H_m and W_m). The data also shows that if H_m exceeds a critical value, none of the *DP* sample will be compartmentalized.

2.2.6 Design Considerations to Maximize f_{total} and R_{total}

So far, our study investigated the effects of changing the dimensions of a straight main channel and the design of the attached bottom well. By optimizing different parameters, sample retention and compartmentalization efficiency of 80-90% could be achieved. To further improve sample compartmentalization into individual droplets with high f_{total} (close to 100%) and high R_{total}, we investigated potential modifications to the main channel geometry. These modifications in the main channel design were based on experimental observations of *DP* breakup during shearing by the *CP* and were aimed at improving the pinching mechanism between adjacent wells (Figure 9a). The main channel geometry was modified to include constrictions before and after each well (well dimensions: $\delta_C = W = l_C = 25$ μm, $W_C = w = 100$ μm; see Figure 13a). To

investigate the effect of the constrictions on the sample digitization, we studied the filling for different *Ca* and compared the results of R_{total} and f_{total} to the studies with straight channels.

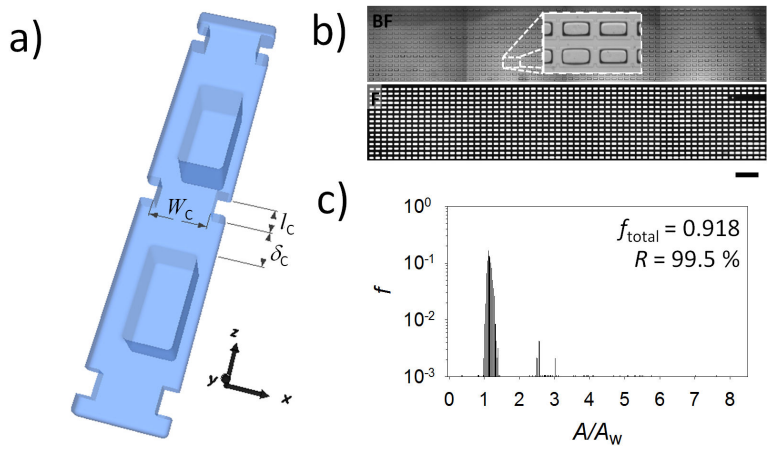

Figure 13. Design considerations to improve sample retention and compartmentalization of individual samples per well. a) Schematic of design modifications to the main channel geometry by placing constrictions before and after each well (δ_C). The constrictions have length of l_C and are spaced apart by W_C. b) Brightfield (BF) and fluorescence (F) images of a 1,024 well chip with constrictions in the main channel ($l_C = \delta_C = 25$ µm, $W_C = w = 100$ µm) which was filled at Ca = 0.004 and resulted in 99.5% sample retention and 91.8 filling efficiency, f_{total}. Scale bar corresponds to 1.0 mm. c) Histogram of the chip shown in (b) based on analysis for singles, doubles, and multi-well filling.

We found that the nicking or breakup mechanism in the inter-well space of the main channel improved dramatically by the use of constrictions. Filling studies at a *Ca* of 0.004 resulted in the 99.5% sample retention (R_{total}) with an f_{total} of 91.8%. In this chip 87.3% of the sample was present as a single droplet ($0.75 < A/A_w \leq 1.50$) and 4.4% of the sample was compartmentalized as sample droplets that remained interconnected through the main channel as

doublets, triplets, or higher order samples ($A/A_w > 1.50$), (Figure 13b,c). The overall trend for a 1,024 well chip in terms of R_{total} was found to be increasing with increasing *Ca* (*i.e.*, 89.8 ± 9.7% at *Ca* 0.004 to 94.5 ± 3.5% at *Ca* 0.020; $n = 2$; Figure 14a). At the same time, the fraction of individual sample compartments (f_{total}) increased as well from 81.3 ± 10.5% (*Ca* 0.004) to 98.0 ± 0.4% (*Ca* 0.020). It was noted, however, that the droplet sizes compartmentalized and retained in each well decreased with increasing *Ca*. This indicated that the improved shearing by the *CP* lead to smaller droplets retained in the wells. In some cases, multiple smaller droplets occupied a single well.

Another design consideration of interest is the number of wells per chip, which effectively defines how much sample can be compartmentalized and analyzed on a single chip. As mentioned in the introduction, different applications may require different numbers of individual samples. While screening assays for drug interaction or sample amplification (*e.g.*, PCR) can be conducted with a few hundred to a few thousand individual samples [53,55], direct evolution studies may require much larger arrays of wells to accommodate up to 10^6 individual samples [80]. We therefore increased the foot-print of our well chips from 1,024 to 10,240 wells per chip to investigate the effect of a 10-fold scale-up. Chips with 10,240 wells were based on the two designs used in the comparative study of straight and constricted main channels. At a *Ca* of 0.010 used for sample digitization we found that the sample retention, R_{total}, was similar in chips with 1,024 and 10,240 wells but overall higher in chips with constricted main channels (Figure 14b).

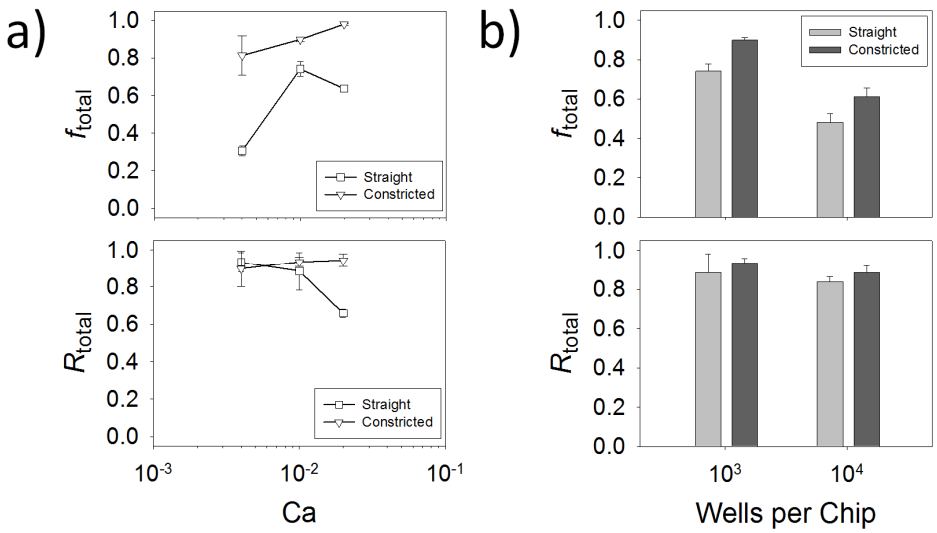

Figure 14. Results of design and scale-up studies: a) Comparison of 1,024 well chips with straight channels (open squares) and constricted main channels (open triangles) based on f_{total} and R_{total} and changing Ca. Note the improvements of constricted channels. b) Effect of scaling from 1,024 wells to 10,240 wells per chip with straight (light grey) and constricted (dark grey) main channels after compartmentalization at Ca = 0.010. Data shown as mean ± SD (n = 2).

The compartmentalization of individual samples (f_{total}), however, decreased with increasing numbers of wells per chip. This result was partly expected and can be attributed to the increasing probability of imperfections in the microfabrication process with increasing area of the feature masters. As a result, some of the main channels connected via bifurcations to the single inlet and single outlet of each chip may experience higher or lower *Ca*, which subsequently affects f_{total} in the respective array of wells along these main channels. The overall trend of improvements in f_{total} and R_{total} for chips with constricted main channels when compared to straight channels was found to be independent from the number of wells per chip (Figure 14b).

The improvements in the compartmentalization of individual droplets per well were mainly driven by the introduction of constrictions in the main channel. The constrictions induce a constrained flow profile after each well. This constrained flow supports the pinching of the *DP* during the shearing process by the *CP*. The filling of wells with *DP* and the subsequent shear off by the *CP*, however, requires continuous flow in the main channel. The flow was induced by a single inlet and distributed to many parallel main channels through the use of bifurcations. The same design of bifurcations was used to recombine the channels into a single outlet (Figure 15a). This design feature, however, had limitations as the chips were scaled up in the number of parallel main channels.

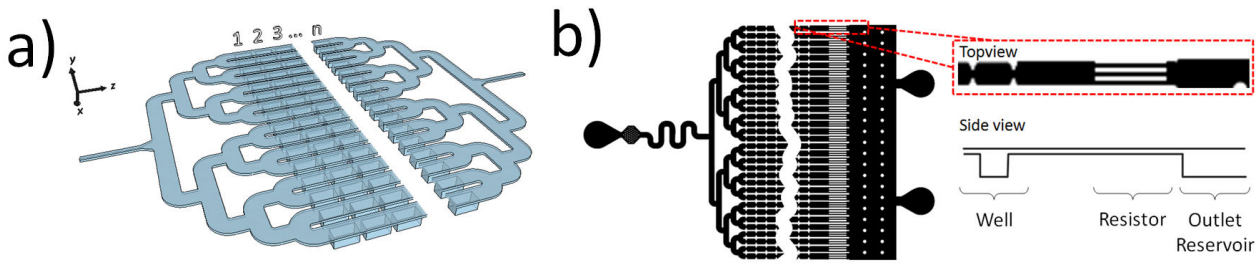

Figure 15. Bottom well chip design used for scale-up. Arrays of wells are created by parallel filling of main channels segments containing n wells. The main channels are connected through bifurcations to a single inlet and single outlet (a). Optimization in the parallel filling of large chips was achieved by leading each main channel outlet into a large reservoir (b).

The increase in numbers of channels filled simultaneously required a highly coordinated outflow of *DP* and *CP* into the single outlet. Some channels experienced higher flow rates for the *CP* and *DP* as result of mismatches in the fluidic resistances between parallel channels. The mismatches in fluidic resistances can be attributed to imperfections in the chip design or chip

fabrication, as well as to variations in the amount of *DP* sample in the channels during the filling of the chip. This ultimately led to the partial filling of *DP* and incomplete compartmentalization of some of the parallel main channels. To address this problem and reduce the interdependence of parallel main channels on equal resistances in the final design, each main channel was connected to a large outlet reservoir (Figure 15b).

In addition, the *DP* pinching mechanism during *CP* shearing was enhanced by *i)* further reducing the constrictions (*i.e.*, from $W_C = ½W_m$ in the results shown in Figure 13 and Figure 14 to $W_C = {}^1/_3 W_m$), *ii)* rounding of the main channel entrance/exit into and out of the constriction, and *iii)* by tapering the bottom wells in flow direction (Figure 16a). The final changes to the bottom well SD Chip design helped to further improve test parameters R_{total} and f_{total}. A typical filling result of a SD Chip with 4,096 wells of approximately 2 nL per well is shown in Figure 16b. Close to 100% of the wells were filled with individual droplets (f_{total} = 98.8%) and the filling showed no dependence on the chip size (Figure 16c,d). The time required to fill these chips was dependent on the total numbers of wells per chip and the sample properties (*i.e.*, *CP* viscosity, surfactant concentration). The time required to fill SD Chips with 1,024 wells was typically on the order of 1-2 minutes, while filling of larger SD Chips (n = 25,600) took between 15-30 minutes.

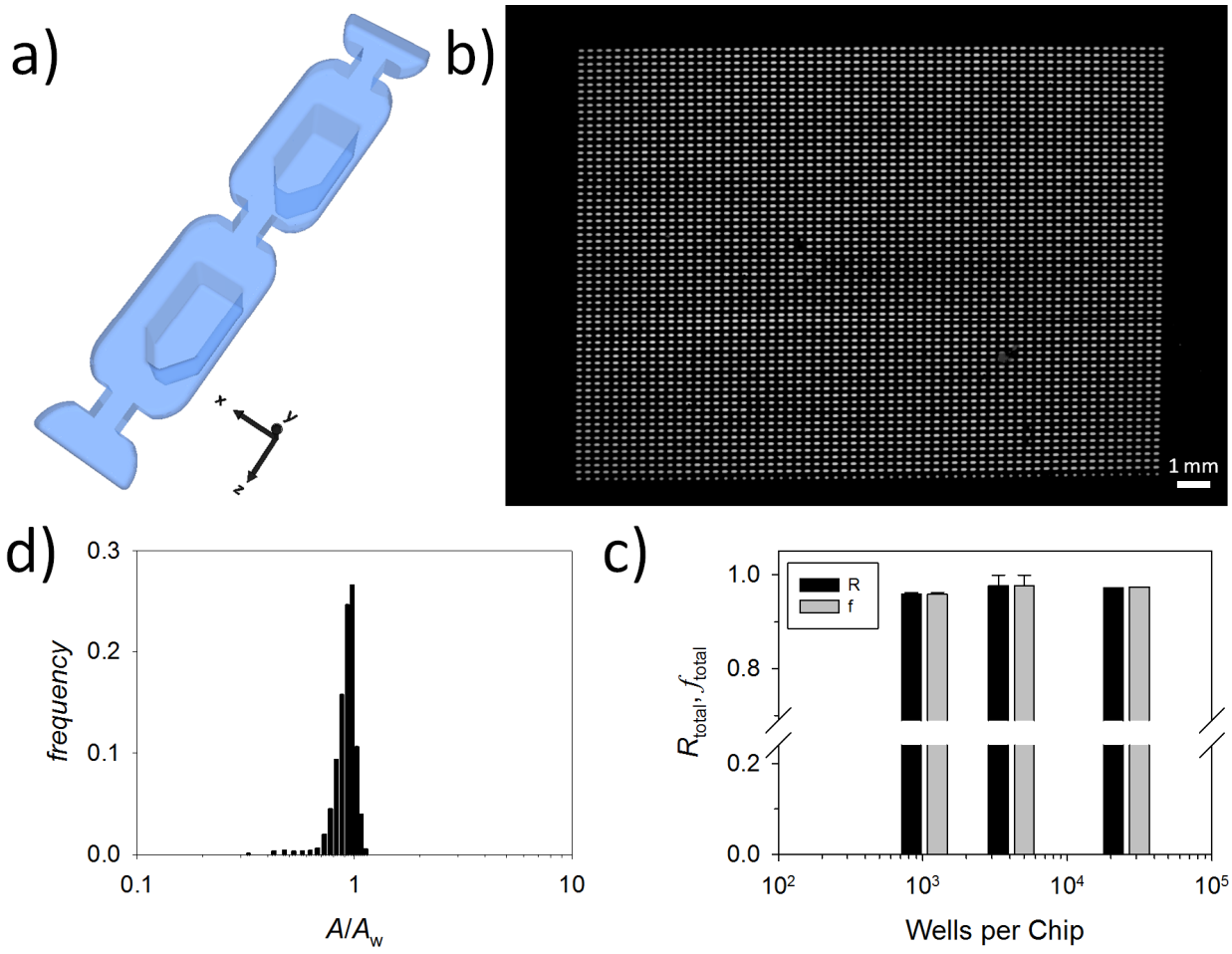

Figure 16. Finalized design of the bottom well SD Chip (a) with in-flow tapered wells attached to a flat main channel with constrictions that are $^1/_3$ of the main channel width. b) Example of SD Chip with 4,096 bottom wells (V_w = 2 nL). The sample retention in this example was 99.9% with 98.8% of the wells present as individual droplets (c). Comparison of sample retention and filling efficiency in bottom well SD Chips with different numbers of wells (1,024, 4,096, 25,600).

2.2.7 Conclusion

A new sample digitization (SD) method was presented and optimized for loss-less compartmentalization of sample volumes in highly dense arrays of microfluidic bottom wells. A parametric study with arrays of 1,024 wells and straight main channels was conducted to investigate how geometric parameters of the microfluidic chip and viscous/interfacial forces of the sample solutions affect the retention and compartmentalization of individual samples per well. We found that a flat and straight main channel with a slight overhang in combination with closely spaced bottom wells can give rise to nearly 80-90% sample retention (R_{total}) and 80-90% of that sample being compartmentalized as individual samples (f_{total}). Design modifications of the main channel (*e.g.*, the use of constrictions in the main channel before and after each well) and tapering the bottom well in flow direction improves the breakup of sample volumes and gives rise to nearly 100% in R_{total} and f_{total}. Furthermore, these results are not limited to scale-up. Bottom well SD Chips with up to 25,600 wells (V_w = 2 nL) allowed for the individual compartmentalization of over 50 µl of sample per chip. These results provide an important foundation for various applications which range from enzymatic studies when used with live cells as single cell microbioreactors to large scale biochemical studies (*e.g.*, drug screening assays).

The microarrays of bottom wells presented in this study allow for the self-digitization of sample volumes in a similar way to those presented in our recent study with microfluidic side chambers [46]. The use of bottom wells, however, provides some features that are more attractive to a wide range of potential applications when compared to side chambers. One of the main advantages in using bottom well arrays is the potential for higher well densities and thus,

allowing larger sample volumes to be compartmentalized per chip for a given area. Furthermore, side chambers confine the sample volume on all six sides, thus increasing the difficulty to remove such samples or components from them (*e.g.*, cells or crystallized structures [46]) by optical [81] or mechanical means [82], if the application requires such measures.

2.3 *Materials and Methods*

2.3.1 Microchip Fabrication

Microfluidic bottom well chips were based on arrays of wells with width (w), length (l), and depth (d) connected to a main channel of height (H_m) and width (W_m=w+2W), where W is the channel's overhang with respect to the bottom well. For the parametric study we varied the main channel dimensions by changing W from 0, 25, 50, to 100 μm and the well spacing, δ, from 50, 100, to 200 μm, while H was 20 μm in all experiments. A sketch of the well chip design is shown in Figure 8a. Arrays of 1,024 wells were used for the parametric investigations. Larger area chips with 4,096, 10,240, and 25,600 wells per chip (V_w = 2 nL) were used in the scale-up studies.

The microfluidic chips were fabricated by multilayer soft photolithography [2] on 3 inch silicon wafers (300-400 μm thick, reclaim; Montco Silicon Technologies, Inc., Spring City, PA) using an epoxy-based negative photoresist (SU-8; MicroChem Corp., Newton, MA). The feature heights were subsequently measured by a custom-built white-light interferometer [83]. Finally, the feature masters and an empty silicon wafer were cleaned with ethanol (200 proof; Decon Laboratories, Inc.; King of Prussia, PA) and silanized (tridecafluoro-1,1,2,2-30 tetrahydrooctyl trichlorosilane; Gelest Inc., Morrisville, PA) under vacuum and overnight.

The microfluidic structures were subsequently cast in PDMS (SYLGARD® 184 Silicone Elastomer Kit, Dow Corning, Corp., Midland, MI). Separately a flat PDMS slab for the inlets/outlet ports was cast on a featureless and silanized wafer. After the PDMS pieces were removed from the masters, inlet and outlet ports were cut into the featureless PDMS slab, the

PDMS pieces were cleaned in with ethanol and blow dried with N_2 gas, and both pieces were placed inside of a plasma cleaner (Expanded Plasma Cleaner/Sterilizer; Harrick Plasma, Ithaca, NY). The plasma cleaner was evacuated thrice (< 100 mTorr) followed by purging with O_2. After the last purge with O_2 and following evacuation below 160 mTorr, the plasma was initiated at high level and left on for 45 seconds. The two PDMS pieces were brought in close contact immediately after removal from the plasma cleaner. Finally, the PDMS pieces were placed at 110-115°C for 24 hours to allow the PDMS convert back to its hydrophobic character.

2.3.2 Sample Preparation

Silicone oil (50 cSt; cat. 378356; Sigma Aldrich, Inc., St. Louis, MO) and mineral oil (30.0 cSt; light, embryo tested; cat. M8410; Sigma Aldrich, Inc.) were used as the *CP*. The silicone oil and mineral oil were supplemented with 0.01%$_{w/w}$ (Gransurf 77; Grant Industries, Inc., Elmwood Park, NJ) and 0.02% (Span 80; Sorbiton monooleate, Sigma Aldrich, Inc.) surfactant, respectively. Highly purified water (MilliQ; Millipore Corp., Billercia, MA) supplemented with 100 μM Fluorescein (Reference Standard; cat. # F-1300; Molecular Probes, Invitrogen Corporation, Carlsbad, CA) was used as the *DP*.

2.3.3 Sample Compartmentalization

Before sample compartmentalization, a long plug of *DP* was sandwiched between *CPs* by aspirating both samples sequentially into PTFE tubing (20G PTFE; cat #50806; Zeus Industrial Products, Inc., Orangeburg, SC). The *DP* plug had a volume of at least 1.5-times the chip

volume. The tubing was connected to the chip's inlet by metal interconnectors (20G ½" blunt, 45°; cat.# NE4520-6; Small Parts, Inc., Miramar, FL) and to pressurized air by LUER connectors (Upchurch Scientific, Inc., Oak Harbor, WA). The air pressure was supplied by a compressor (Panther, # P100-24AL/M07090; Werther International Inc., Houston, TX) and regulated by a pressure gauge (0-100 psi, AR91-100; Omega Engineering, Inc., Stamford, CT).

The chip filling and compartmentalization was visualized by a wide area microscope (AZ100 Multizoom; Nikon Inc., Melville, NY; Zoom Stereo Microscope SZ61; Olympus Imaging America Inc.; Center Valley, PA) equipped with a 1× and 4× objective (NA: 0.1/WD: 35mm and NA: 0.4/WD: 20mm, respectively; Nikon Inc.) in bright field and under fluorescence excitation (FF01–482/35–25, FF01–536/40–25; SEMROCK Brightline, IDEX Corp., Rochester, NY). Images were acquired using a CCD camera (GC1380; Allied Vision Technologies Canada Inc., Burnaby, B.C., Canada) and custom coded acquisition software (LabVIEW v8.6; National Instruments Corporation, Austin, TX).

2.3.4 Computational Fluid Dynamics (CFD) of Sample Compartmentalization

Three-dimensional multiphase fluid simulations of the sample compartmentalization in a single side chambers and bottom wells were conducted with a CFD package (Fluent, Version 6.3.26; Fluent Inc.; ANSYS, Inc., Lebanon, NH). The droplet compartmentalization was simulated for different *Ca* and varying dimensions of the main channel (W_m, H_m) with a 100 µm × 200 µm × 100 µm ($w \times l \times d$) bottom well. The designs were converted into finite elements using a hexahedral meshing strategy with a resolution of 2.5 – 5.0 µm between node points. Water (ρ = 998 kg m^{-3}, μ = 1.003×10-3 kg m^{-1} s^{-1}) and silicone oil (50 cSt; ρ = 980 kg m^{-3}, μ =

0.049 kg m^{-1} s^{-1}) were used as *DP* and *CP*, respectively, in all simulations. The model solver was defined as pressure-based, with a 3-dimensional and implicit formulation, unsteady with non-iterative time advancement, with an absolute velocity formulation, and a first-order implicit unsteady formulation.

A volume of fluid (VOF) solver was used for the multiphase model with two phases, explicit VOF scheme, and a Courant number of 0.25. The phase interaction was defined with wall adhesion properties and different γ values for the water-oil interface ranging from 5-30 mN m^{-1}. The boundary conditions were set as follows: The single inlet was defined by a flat velocity profile with a linear flow velocity ranging from 1 to 8 mm s^{-1}; the outlet was defined as outflow with a constant pressure ($P_{Outlet} = P_{atm}$ = 101 325 Pa); and the walls enclosing the main channel and well were set to have a hydrophobic contact angle of 175°. The main channel and bottom well were then "pre-filled" with the *CP* and *DP* using Fluent's "Adapt" tool resulting in a *DP* plug with a volume of 1.5 – 2.0 times V_w and reaching up to 25 µm before the well. The fluid flow profile and the volume fractions were then simulated with fractional steps for the pressure-velocity coupling. The spatial discretization was implemented by a first-order upwind scheme for the momentum and a pressure staggering option (PRESTO!) set for the pressure. The volume fraction was discretized using the Geo-Reconstruct option. All residual tolerances were set to 0.001. The simulations were subsequently iterated with time steps ranging from 0.1 to 5.0 µs.

2.3.5 Data Analysis & Statistics

Data analysis was conducted from fluorescence images of the entire SD Chip. A custom programmed matching algorithm was used to stitch individual images taken from large area chips (LabVIEW v8.6; National Instruments Corporation). A separate custom LabVIEW program was then used to analyze the fluorescent image using blob analysis [84], a user specified well size (taken from the brightfield images), and two different thresholding schemes. The 8-bit images of the fluorescent *DP* retained in the wells and main channels showed different grey levels (range 0-255). The fluorescent sample in thin main channel had much lower pixel grey level intensities than fluorescent sample in the much deeper bottom wells. This difference in grey level intensities allowed two thresholding schemes for the analysis. These thresholding schemes were used to calculate *i*) the filling efficiency and *ii*) the retention ratio. The filling efficiency is based on the analysis at low threshold of individual compartmentalized samples (*i.e.*, accounting for wells which remained interconnected by a *DP* thread in the main channel). The retention ratio is based on the image analysis at high threshold to account for the total number of wells filled (i.e., retained) per chip regardless of well interconnection by the *DP* in the main channel. Therefore, our analysis and data representation will be based on *i)* the fraction of individually compartmentalized samples per chip (or compartmentalization efficiency), f_{total}, and based on *ii)* the total sample retention per chip, R_{total}. An example of the data representation for f_{total} is given in Figure 17.

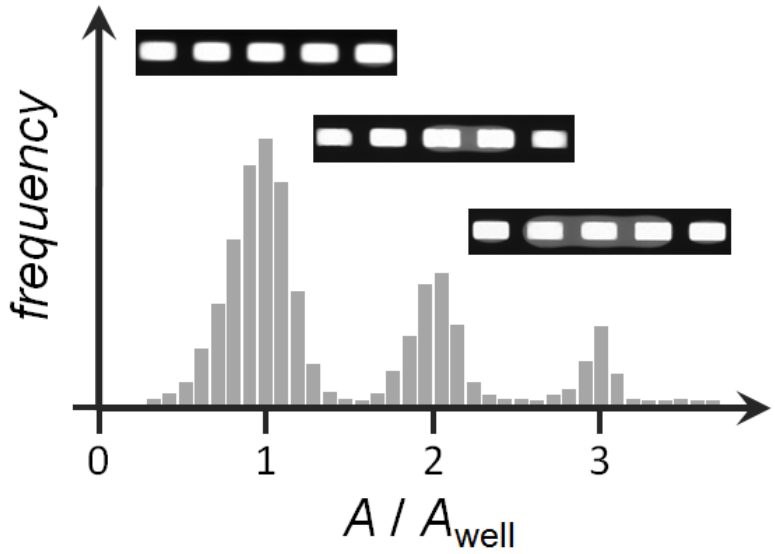

Figure 17. An example of data representation for compartmentalization efficiency based on the LabVIEW analysis. The image analysis distinguishes individually compartmentalized droplets and droplets that are connected through the main channel. The area of the droplet is normalized to the area of a single well (x-axis) and given as a frequency distribution.

CHAPTER 3

DROPLET REMOVAL STUDIES

3 Sample Manipulation and Removal Studies

Droplet compartmentalization and digitization was shown in the previous chapter to be a versatile technology to separate a sample into hundreds or thousands of nanoliter-sized reactors. Current SD Chips based on side chambers have been used for biological applications such as dLAMP and crystal growth studies [46,47]. The unique features of the bottom well SD Chip design provide a foundation for a variety of other applications. These applications include those that require longtime monitoring of reaction kinetics or growth patterns of biological samples in droplets (*e.g.*, isolation of monoclonal cells for antibody production), which can be accomplished in specially designed perfusion based microfluidic chips. Some applications, however, may require further interaction with the digitized droplets or the targeted removal of specific droplets. These droplets may contain samples of interest and are subject to further analysis (*e.g.*, a rare tumor cell, an amplified sample). In order to enable such interactions on our SD Chip platform, different strategies were investigated that showed potential to accomplish the active interaction and removal of droplets directly on chip. These methods are conceptually summarized in Figure 18 and include *1)* Droplet Removal By Thermocapillary Flow and Optical Tweezers (Figure 18a-d), *2)* Droplet Removal By Mechanical Means (Figure 18e-h), *3)* Droplet Removal By Thermal Bubbles (Figure 18i-l), and *4)* Droplet Removal By Micropipetting (Figure 18m-p).

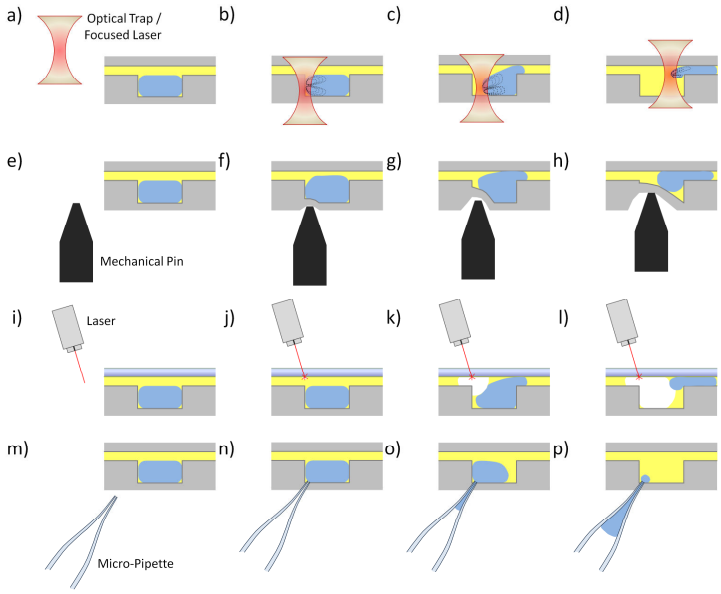

Figure 18. Conceptual depictions of removal methods of aqueous samples (blue) compartmentalized in an oil phase (yellow). The sample is first compartmentalized and after the flow is stopped, the following methods may be used: (a - d) Droplet removal by thermocapillary flow induced motion of a confined droplet. A focused laser is positioned to interact with the interface of an aqueous droplet in oil. The localized heating at the interface leads to a localized change in surfactant concentration, which subsequently results in flow patterns inside and outside the droplet that can be used to move a droplet. (e - h) Droplet removal by deformation of the substrate using a mechanical pin. The cavity confining a compartmentalized droplet is deformed and results in the forced movement of the droplet into the main channel. (i - l) Generation of a cavitation bubble by localized heating at a surface with absorption difference. The strong heat gradient results in the formation of an air bubble which is then pushed towards the droplet and results in its deformation and displacement. (m - p) Droplet aspiration and removal using a micropipette. The substrate is penetrated by a micropipette to controllably remove a droplet by aspirating its contents.

3.1 *Introduction and Background*

3.1.1 Droplet Removal By Thermocapillary Flow and Optical Tweezers

Droplets immersed into an immiscible fluid, also known as emulsion systems, are often free flowing and easily manipulated by mechanical stirrers and tweezers. A direct interaction between a droplet and the surface of a stirrer can be disadvantageous if potential cross-contamination between droplet and stirrer is to be minimized. A contactless interaction with a droplet or particle can be achieved by tightly focusing light of a given wavelength at the sample. This was first shown on a micrometer scale with solid particles in water in the 1980's[85]. Since then the field has greatly matured and these 'optical tweezers' are used today for the manipulation of particles, droplets, and aerosols in a variety of chemical and biological systems [86].

A tightly focused laser can also be used to induce localized heating at the interface of two immiscible phases, which results in the generation of surface tension gradients. The differences in surface tension lead to fluid motion in an effort to equilibrate the system. This phenomenon is called Marangoni flow [87] and has been discussed in early literature [88]. The forces associated with such flows are small (on the order of tens of nN [89,90]) and have only recently become of interest with the advent of microfabrication and microfluidics. Taking advantage of these effects, microfluidic studies with tightly focused lasers were shown to actively stop the flow of droplets (Figure 19b)[90,91] and to actively switch or alter the flow direction of unconfined droplets [91]. The latter study has great potential as a microfluidic sorting tool [92]. The forces associated to stop the flow of droplets shown in these examples were estimated to be approximately 180 nN with an average heating time required at the interface of 4ms [90].

We investigated the feasibility to use such optical tools (*i.e.*, optical tweezers and thermocapillary flow induced motion) to move and actively transport droplets compartmentalized and confined in our SD Chips. In order to accomplish this we built a single optical tweezers setup to study the potential of inducing thermocapillary flow in droplets compartmentalized in different SD Chips.

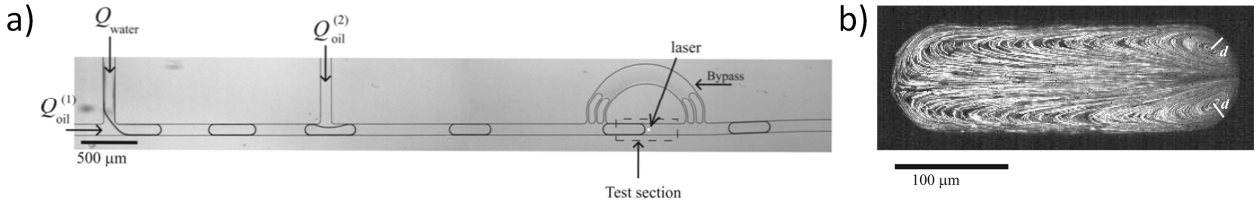

Figure 19. Thermocapillary flow was shown to slow down and stop droplets (a). The mechanism induces an internal flow pattern in the droplet, shown here by tracer particles, which effect its motion inside the microchannel (b). Reprinted (adapted) with permission from [90]. Copyright (2009) American Chemical Society.

3.1.2 Droplet Removal By Mechanical Means

PDMS is one of the most commonly used substrates for microfluidic devices. This is mainly due to the many advantages of PDMS for microfluidic applications, including transparency, chemical stability, and flexibility. The latter property has been successfully applied to applications requiring valving [93] and is conceptualized in Figure 20a. In this simplified example, two channels are layered perpendicular and on top of each other, separated only by a thin PDMS membrane. A valving channel (white in Figure 20a) is pressurized resulting in the deformation of the membrane at the intersection of the two channels and effectively closing the

sample channel where it intersects with the valving channel. This concept has been used for large-scale integration in microfluidic chips to study complex binding kinetics (Figure 20b) [94,95]. PDMS is an ideal substrate for membrane valves and has an average stiffness or Young's Modulus (*E*) of 955 kPa and 266 kPa, when used in the recommended base to catalyst ratio of 10:1 or at a higher ratio of 20:1 [96], respectively. For comparison, *E* for a cancer cell is on the order of 0.2-4 kPa [97] while *E* for stainless steel was found to be 180 GPa [98].

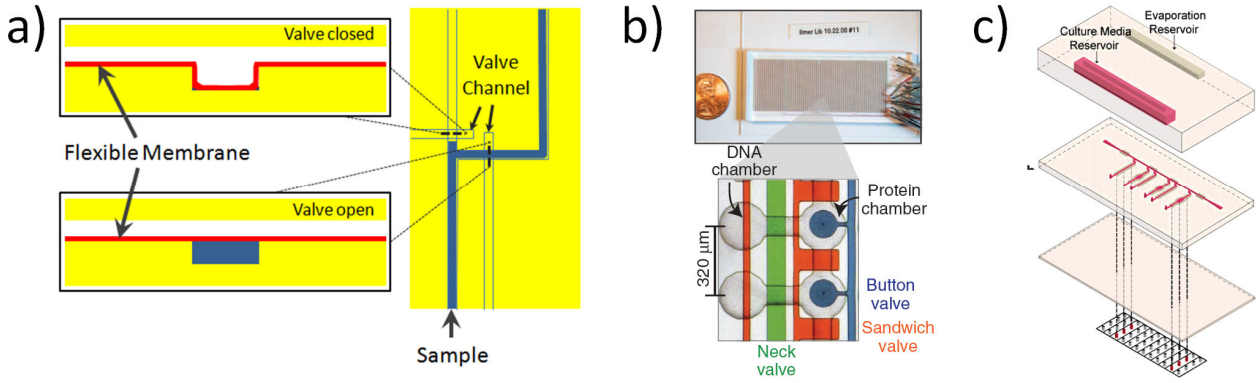

Figure 20. Examples of applications with flexible membranes: a) Concept of valving using a flexible membrane in microfluidic chips and a pressurized valve channel. This method has been used in large scale integration microfluidic chips for antibody binding affinity studies (b). Reprinted (adapted) with permission from [94]. Copyright (2010) Nature Publishing Group. The flexibility of the PMDS substrate has also been used for pumping using mechanical pins from Braille displays (c). Reprinted (adapted) with permission from [82]. Copyright (2005) American Chemical Society.

The flexibility of PDMS substrates has also lead to the use of addressable micropins in Braille keyboards for membrane deformation. Braille keyboards are commonly used by blind or visually impaired people to read by touching a micropatterned surface. Takayama and colleagues pioneered the use of this technology for microfluidics with particular focus on applications requiring pumping and valving in on-chip cell culture applications (Figure 20c) [82,99,100]. The group used Braille pins with diameters of 900 μm and reported forces applied across thin PDMS membranes of approximately 0.2 N [99]. Using this method, the group was able to control the flow in their microfluidic chips for several weeks.

The use of micropins for sample interaction has the advantage of no direct contact with the sample. Limiting direct sample interactions reduces the risk of cross-contamination. The wells and droplets in our SD Chips are typically on the order of 50-100 μm in diameter and would require much smaller pins than those used in commercial Braille keyboards. We were interested in investigating the use of mechanical forces, applied externally to the SD Chip, for droplet removal from the well and subsequent transport on chip.

3.1.3 Droplet Removal By Thermal Bubbles

Localized heating of a substrate can result in boiling at its surface and the generation of a thermal bubble. Boiling occurs on surfaces in stages and is used in fields of metallurgy and fundamental studies on heat transfer. When heating a surface that is in contact with a liquid, a transition occurs over time between the local heat transfer coefficients (HTC). A vapor layer forms at the interface between the liquid and the solid, when the difference in HTC between the two interfaces exceeds a specific critical heat flux (CHF). The resulting insulation layer grows with increasing surface temperature forming a bubble (Figure 21) and can lead to a dry-out of the surface. The heat transfer between substrate and liquid is strongly effected by surface patterns, surface material, and surface hydrophobicity [101].

Bubbles generated at a surface can act as microfluidic valves by blocking off flow in microfluidic channels. They also can be used as pumps by sequential heating which results in the expansion and contraction of the bubble [102].

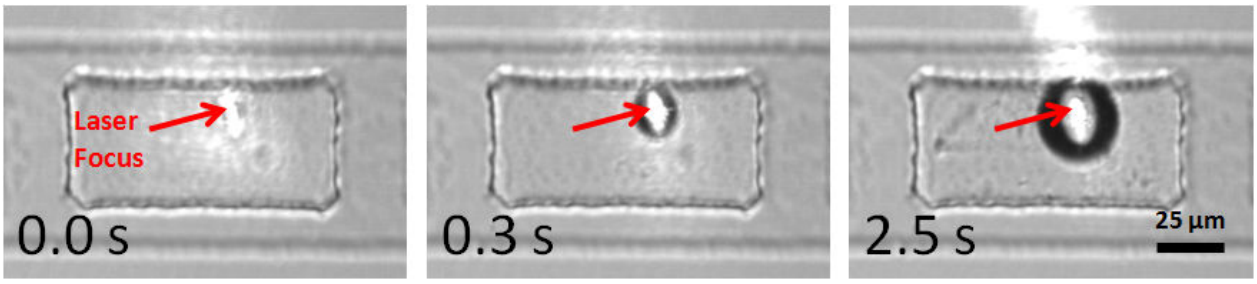

Figure 21. Example of the cavitation bubble formation in a hybrid oil-filled microfluidic SD Chip. A 1,064 nm laser (1.5 W) was focused at the surface of a thin ITO coated cover glass bonded to a PDMS channel.

Metal films are often used as a mediator either for resistive heating or heat generation through absorption when induced by a laser. The latter approach appears more elegant as it minimizes the need for complex circuitry and allows a fast, localized, and non-invasive heating that is defined by the laser intensity and spot size. This method has previously been shown to be a versatile tool for surface cleaning and for the generation of complex microfluidic flow patterns on a time scale of μs [103,104]. Thin metal films deposited on glass provide sufficient absorbance to generate heat for cavitation bubbles. In many microfluidic studies, indium tin oxide (ITO) was found to be a suitable substrate, due to its good optical transparency and well characterized electrical properties [105-107]. ITO is known to absorb across a wide spectrum of light and to have a weak absorption in the infrared range (absorption coefficient for 1,047 nm: 2×10^{6} m^{-1} [108]), which is ideal for our optical setup, as the weak absorption allows precise control over heat generation.

We expanded on these studies to investigate the feasibility to use cavitation bubbles to transport confined droplets in our digitization chips. In order to conduct the study, a modified SD Chip was constructed, which consisted of a hybrid ITO-glass-PDMS structure.

3.1.4 Droplet Removal By Micropipetting

All three previously shown methods for droplet interaction and droplet transport are non-invasive. Micropipetting in contrast to these methods is an invasive method. In order to access the droplet a pipette has to first penetrate the PDMS substrate close to the desired droplet to be removed. Subsequently, the pipette directly interacts with the droplet by aspirating it and extracting it from the confinement of the microwell (Figure 18m-p). This method has several advantages over the on-chip manipulation: *i)* the droplet and its components can be controllably aspirated and removed, *ii)* there is limited potential for sample destruction due to heat during the removal, and *iii)* the extracted droplet can be directly transferred and applied to other sample analysis methods (*e.g.*, Mass Spectrometry).

The use of micropipettes for scientific applications dates back almost 200 years. Custom made micropipettes were most notably used by famous French chemist and microbiologist Louis Pasteur [109]. Micropipetting, especially with custom made pipettes from pulled glass capillaries have found applications for studies on single cells [110,111] to molecular analyses by mass spectrometry [112,113]. We were interested to use custom pulled glass capillaries to aspirate nL sized droplets from our SD Chips.

3.2 *Results and Discussion*

3.2.1 Droplet Removal By Thermocapillary Flow and Optical Tweezers

Thermocapillary flow induces a localized fluid motion at the interface of two immiscible fluids. This motion has been used to slow down or repel droplets that are partially unconfined (*i.e.*, constrained in its shape by channel walls) and already in motion [90,91]. We were interested in using this phenomenon to induce motion in a stationary droplet that is confined by the channel walls of the SD Chip and constrained in its shape. The goals of this project were *i)* induce flow inside a confined droplet by a laser, *ii)* take advantage of the induced flow to force the droplet out of the well, and/or *iii*) to investigate alternative methods that use optical tweezers to remove droplets from well.

In a previous study we investigated the use of optical tweezers for the active manipulation of microparticles as vehicles to allow the parallel delivery of biological stimuli [81]. For these studies we built two optical setups to allow the use of a tightly focused laser as an optical tweezers. A sketch of the setup is shown in Figure 22. The two setups were similar except for the use of different lasers (Setup 1: 532 nm, Setup 2: 1,064 nm) and the use of a spatial light modulator (SLM) in Setup 2 in place of the stirring mirror in Setup 1 (see Figure 22a). The use of a SLM as a stirring mirror allows generating large arrays of individually addressable focal spots in the image plane at the same time [114], while a single stirring mirror allows only a single foci.

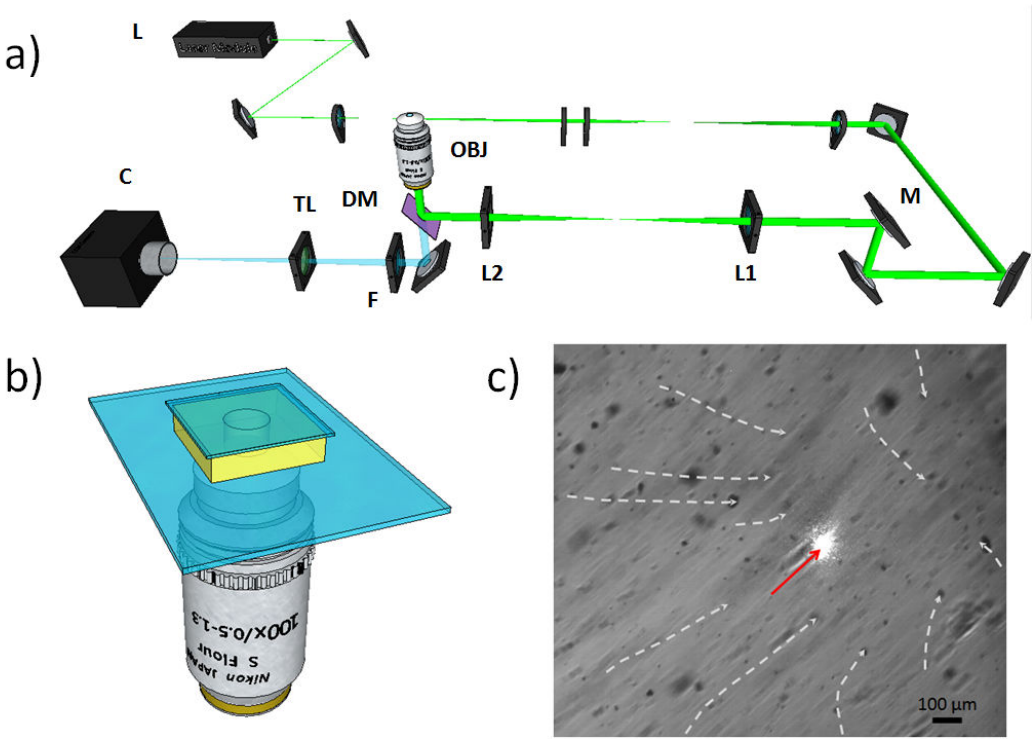

Figure 22. Drawing of a setup used for thermocapillary flow and optical tweezers studies (a). A laser (L) is expanded in a Keplarian telescope lens system and stirred by a mirror (M) through lenses (L1, L2) into the back aperture of a microscope objective (OBJ). A dichroic mirror (DM) is used to transmit the light of the imaging system (not shown) and to reflect the laser light. A filter (F) is used to eliminate unwanted light before the image is projected onto a camera (C) by a tube lens (TL). In setup 2 the stirring mirror (M) before the 4f lens system (L1, L2) is replaced by the spatial light modulator. b) Sketch of the simple PDMS slab used for the initial studies. c) Results from laser induced flow in 50 cSt silicone oil supplemented with 0.1 mg/g Oil-Red-O dye. The laser focus on the cover glass is indicated by the red arrow. Tracers of particles (white dashed lines) are shown for the duration of 15 seconds after the laser was switched on.

Initial studies were conducted with lipophilic dyes that had strong absorbance in the spectral range of the the laser used in setup 1. The main hypothesis behind the use of dyes for our droplet removal study was the potential increase in laser absorption in one of the two phase materials (*i.e.*, oil or water) with the result of enhancing the fluid motion. To minimize effects of interactions with the aqueous sample we focused on improving laser absorption in the oil phase. However, there were no suitable lipid dyes available that indicated high absorbance in the near infrared spectrum for the laser used in setup 2. As a result we conducted the absorbance study with the 532 nm laser on setup 1. Oil-Red-O, a lipophilic dye, was found to be a suitable candidate for this study and we first investigated the laser induced fluid motion in the simple PDMS well slab (Figure 22b). We found that strong fluid motion was induced when the laser was focused at the interface of oil and glass (Figure 22c**)**. Subsequently, a SD Chip was used to compartmentalize an aqueous sample and using a 0.01 mg/g Oil-red-o in oil solution as the *CP*. The use of the dye, however, had the side effect of accumulating at the PDMS surface of the SD Chip, rendering the chip red. The subsequent droplet removal study was unsuccessful. The compartmentalized droplets showed no deformation or any motion that would indicate potential removal of the droplet using that experimental setup. The use of a single laser focus also limited the interaction between laser and droplet. The sample stage had to be moved in Setup 1 using a translation stage to achieve relative motion between the stationary laser and a compartmentalized droplet.

Earlier studies with cells and particles as carriers for potential biological stimuli showed the feasibility of Setup 2 which employed the SLM. As a result, subsequent studies were conducted with multiple foci on setup 2 with a 1,064 nm laser and without lipophilic dyes in the *CP*. Different experiments with bottom well and side chamber SD Chips were conducted and

showed no success inducing motion and removing fully confined droplets. In a separate study a side-chamber SD Chip was used to compartmentalize an aqueous PCR mix in light mineral oil. As it was expected from the higher surfactant concentration, the droplet compartmentalization resulted in droplets that filled out the entire chamber and smaller droplets that were only partially confined. Similar to the previous studies we observed no laser induced motion in fully confined droplets. However, it was found that small droplets (*i.e.*, 10 – 20 µm in diameter) could be slowly moved by the laser. The laser was focused at the oil-water interface on one side of the droplet and this resulted in a slow motion forward (*i.e.*, away from the laser). The droplet was not attached completely to the surface. Other small and unconfined droplets showed induced motion by the laser. However, the size of the droplets prevented them to be transported out of the side chamber as the force by the laser to induce droplet motion was insufficient to deform the droplet (*i.e.*, squeeze the droplet into the thinner main channel (Figure 23).

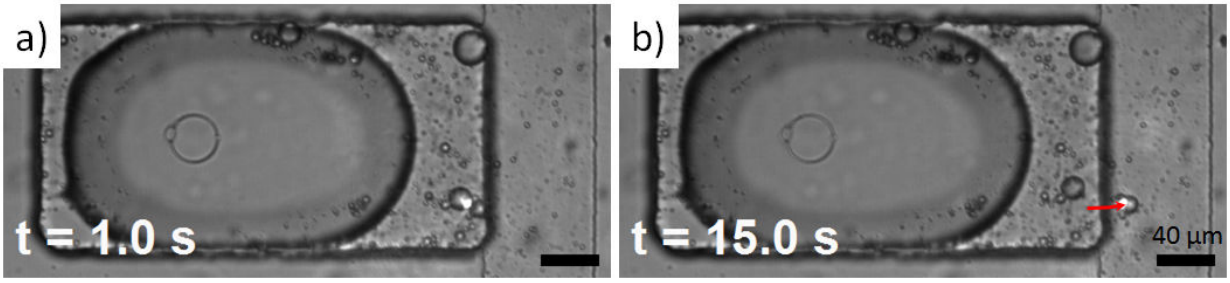

Figure 23. Images showing the active removal of a small aqueous droplet from a side chamber of a SD Chip using setup 2. Note the slow displacement of the droplet indicated by the red arrow in b). The images show a 200 µm wide, 400 µm long, and 100 µm deep side chamber adjacent to an 80 µm wide and 20 µm tall main channel.

The slow induced motion of small droplets shows a limited applicability of this method to actively transport droplets out of the wells. Another application of optical tweezers is the active capture and transport of small specimen (*e.g.*, cells or particles). An aqueous sample was spiked with mouse B-cells and compartmentalized in a bottom well SD Chip. The optical tweezers of Setup 2 were then used to capture and transport the cells to the water/oil interface of the droplet. Cells can be actively transported to the droplet interface and brought in close proximity using multiple foci at the same time (Figure 24). The strength of the optical tweezers was insufficient to force the cell out of the droplet and into the oil phase or the neighboring droplet. The captured cells, however, enabled the moving of the droplet by dragging the cell along the droplet interface. However, it was not possible to force the droplet outside the well by this method.

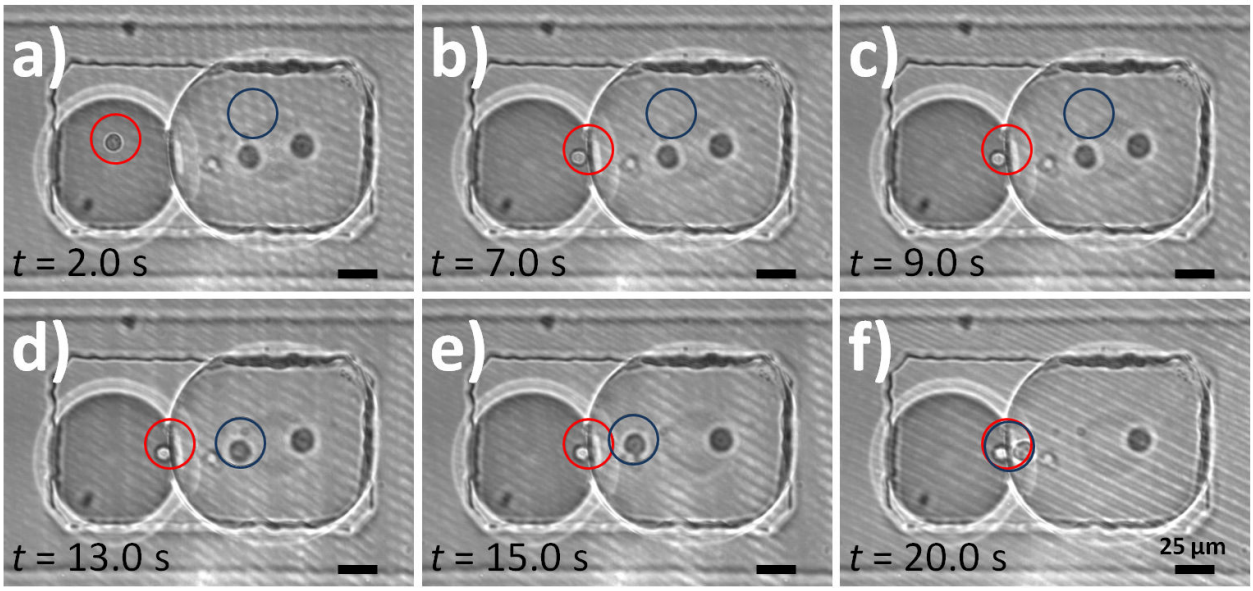

Figure 24. Example of the use of optical tweezers for the capture and active transport of B-cells inside droplets. The images show two droplets confined in a bottom well, each containing B-cells. Single foci (red and blue circles) are used to first capture and subsequently transport a cell to the interface between the two droplets.

3.2.2 Droplet Removal By Mechanical Means

Micropin studies were conducted with a blunted needle tip made from a hypodermic metal needle. The needle was attached to a 3-dimensional translation stage and positioned so that the movements of the needle can be visualized with respect to the microfluidic SD Chip (Figure 25). After compartmentalization of the aqueous sample in the SD Chip, the chip was turned bottom up and placed on the sample table of a microscope. The microneedle was positioned relative to the SD Chip so that the needle tip was in close proximity of a bottom well containing a compartmentalized droplet.

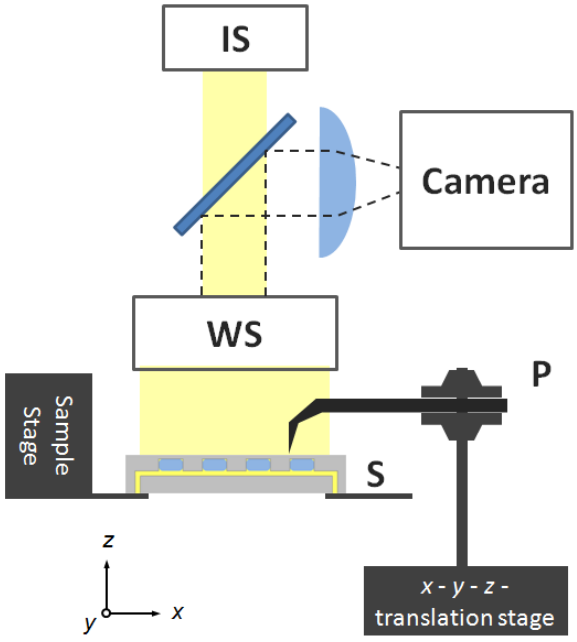

Figure 25. Sketch of the experimental micro-pin setup. The microfluidic chip (S) and the tip of a micro pin (P) are visualized by a zoom scope. The scope has a wide area lens system (WS) and an illumination system (IS) for brightfield and fluorescence imaging. The micro pin is fixed in a 3-D micro-translation stage to allow precise movements of the pin with respect to the microchip.

The micropin was gently moved facilitated by the micro-translation stage to push against a thin PDMS membrane separating the droplet and the needle tip. A sequence from movies acquired during the experiments is shown both by brightfield and fluorescence microscopy in Figure 26. The microneedle was slowly pressed into the PDMS bottom of the SD Chip, which resulted in the expected deformation of the well. The droplet inside the microwell deformed also and squeezed out of the well. The droplet was increasingly forced out of the well with increasing force applied to the chip bottom.

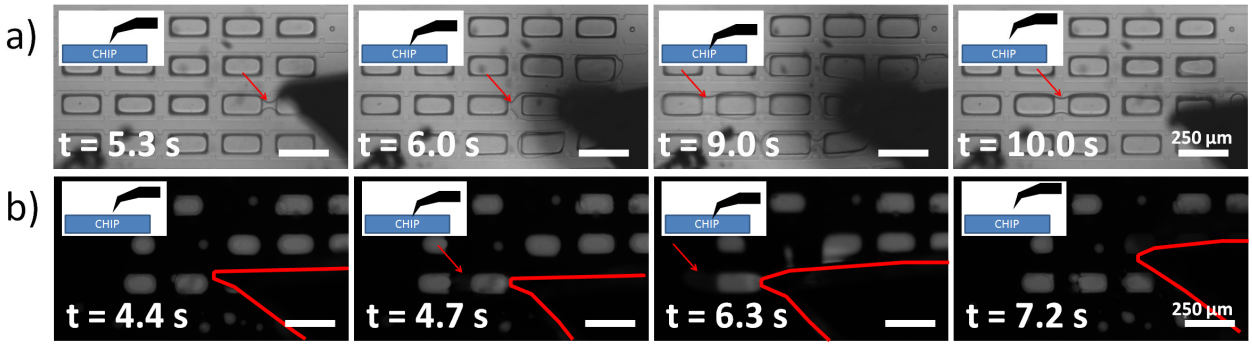

Figure 26. Brightfield (a) and fluorescence (b) microscopy image sequence of droplet studies with a micropin. The insets show the position of the micropin with respect to the SD Chip surface. Note the interconnection of neighboring wells with increasing force of the mirconeedle on the SD Chip (red arrows).

When the removed droplet reached an adjacent well that contained another droplet, the droplets started to fuse and form interconnecting bridges of aqueous phase (see red arrows in Figure 26). When the force of the microneedle tip was subsequently reduced and the tip was removed from the PDMS bottom, the chip regained its original shape and the droplet retreated

back into its original well. After completion of the micropin studies, some of the droplets that were originally confined to a single well showed bridging through the main channel to neighboring wells and droplets. This bridging indicates that fractions of the disperse phase were separated from the original droplet during the deformation of the PDMS chip and the squeezing of confined droplets out of the wells. Overall we found from our study that mechanically induced squeezing action can only be applied to SD Chips that had a thin membrane, either as the top or as the bottom of the chip. The latter design was used in all studies as it was expected that the mechanical action applied to the bottom of the wells will be most effective for droplet removal. However, the use of mechanical pins with a tip size of 50-100 μm as used in the present study has also the potential of damaging the thin membranes.

Our study showed that strong adhesion exists between the droplet and the substrate of the microfluidic SD chip. This adhesion is reflected in the retreat of the droplet into the well upon removal of the micropin from the bottom of the chip. Takayama and colleagues used micropins that had diameters of 0.9 mm and estimated the forces they could apply onto the substrate to be approximately 0.2 N**[99]**. The blunted needle tips used in our study were much smaller and had a diameter of 50-100 μm. The smaller needle tip allowed precise positioning on 2 nL wells but also resulted in partial penetration of the thin PDMS membrane after applying multiple cycles of pressure and release action by the micropin setup.

3.2.3 Droplet Removal By Thermal Bubbles

Thermally induced bubbles provide a versatile method for droplet removal. A substrate with a thin metal film is needed to induce sufficient heat by a laser at the interface between the substrate and a sample solution. Indium-tin-oxide is an ideal test material as it transmits approximately 80% of the light at a wavelength of 1,064 nm [115]. The remaining 20% of the incident light will be both reflected and absorbed by the material. For our study it can be assumed that the greater fraction of the light that is not transmitted will be absorbed. The low absorbance was used as an advantage for the thermal bubble studies as it allowed precise control over the energy delivered to the metal film by adjusting the laser power. As a result the experimental setup provided sufficient control over bubble generation, growth, and direction when moving the thermal bubble. For all the experiments in this study a customized laser setup was used that employed a 1,064 nm laser, a *4f* optical trapping setup, and spatial light modulator to actively control the position and direction of a focused laser beam in the image plane of the sample.

In order to study the effect of a thermal bubble on droplet removal in the SD Chip, we had to first create a hybrid PDMS-ITO chip. Holes for the inlet and outlet ports were carefully drilled mechanically into an ITO coated glass slide. The microfluidic section of the chip (**Figure 27b**) consisted of a PDMS cast that contained the channel structures. Separate PDMS slabs containing through holes for the inlet/outlet ports were subsequently sealed to an ITO slide together with the PDMS cast. The PDMS inlet/outlet port slabs were necessary to facilitate the filling of the chip during compartmentalization of the sample.

Initial studies were conducted with both standard, uncoated glass slides and ITO coated glass slides. The laser setup used for the thermal displacement studies was the same as the setup that was used in the optical tweezers studies. This setup allowed precise control over the focal position of the laser based on user specific coordinates on a computer screen. Different power settings for the 1,064 nm laser were used to investigate the controllability of thermal heating. A water droplet was placed on the cover slides and the laser was then focused near the water/air interface (red circle in Figure 28a,b).

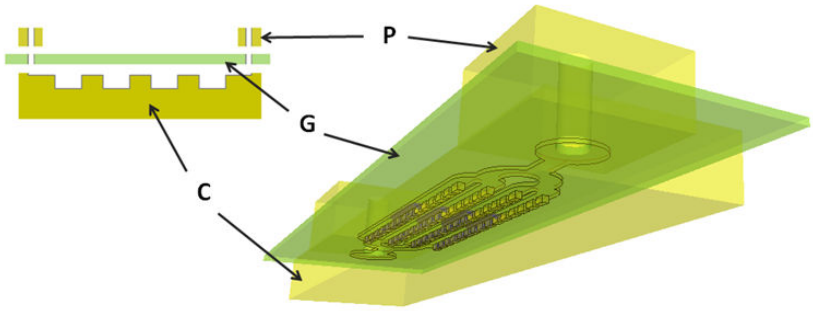

Figure 27. Chip design used for droplet removal by thermal bubbles. The chip consists of an ITO coated glass slide (G) with through-holes for the inlet ports. A cast of the channel structures (C) and separate slabs with inlet/outlet ports (P) made from PDMS are aligned and sealed to the ITO glass slide.

Small bubbling could be observed in experiments with ITO cover slides when the laser was switched on. The bubbling resulted in a displacement of the water/air interface, d_L, which was measured over time (Figure 28c). No bubbling or displacement of the interface was observed when uncoated glass slides were used. The experiments with ITO slides showed good control of the thermal heating. The amount of interface displacement could be controlled with

changes in laser power on a reasonable timescale to allow for additional tasks such as moving the laser focus in the image plane to interact with droplets in the wells of an SD Chip (Figure 28c).

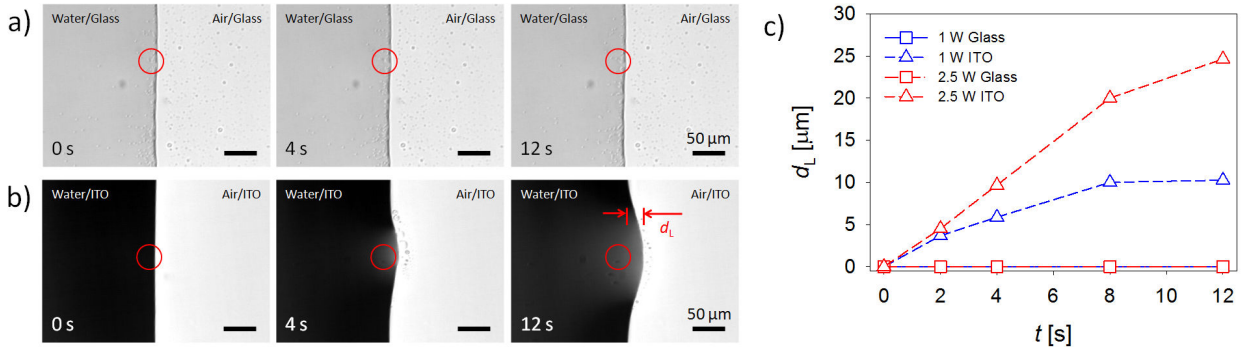

Figure 28. *Laser induced heating near the water/air interface on uncoated (a) and ITO coated (b) glass cover slides. A 1,064 nm laser was used at 1 W and 2.5 W power (a, b). The laser focal point is indicated by a red circle. The displacement of the interface, d_L, due to laser induced heating and bubbling at the glass surface was measured over time (c). A strong interface displacement dependent on laser power was observed on ITO covered slides while glass slides showed no displacement.*

Subsequently, hybrid ITO-SD Chips were used for thermal displacement studies (Figure 27). Low viscosity silicone oil (5 cSt) with high surfactant concentration ($1\%_{w/w}$ Gransurf 77) was used for droplet compartmentalization. The droplet compartmentalization resulted in a filling efficiency, *f*, of 89.6% with a filling ratio of individual wells, *R*, of 90.6%. More than a quarter of the filled wells (27.3%) contained droplets with less than 75% normalized cross-sectional areas (A/A_w), indicating that the compartmentalized droplets were made up of smaller emulsified droplets. This result was intended as preliminary studies indicated that smaller droplets (*i.e.*, those not completely confined to the well) were easier to move by the laser-

induced bubbles. In order to simplify the further discussion of the results we will refer to the cluster of droplets in the following example as a single droplet.

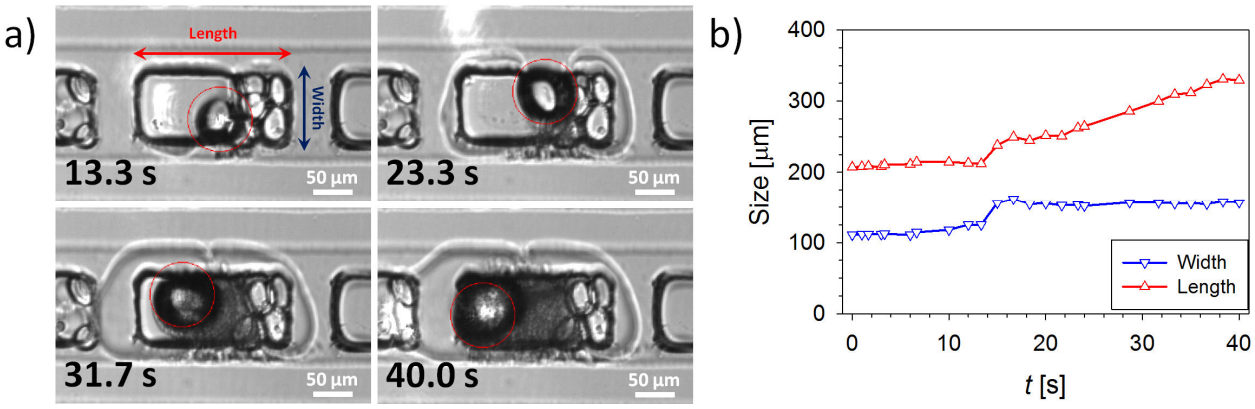

Figure 29. Sequence of images from studies with thermally induced bubbles to interact with confined droplets (a). Shown is a 2 nL well filled with an emulsion of aqueous droplets covered by 5 cSt silicone oil. A 1,064 nm laser was used with the power set to 3 W and focused at the glass-oil interface (red circle). The thermal bubble was grown within seconds and used to push the droplet out of the bottom well. The changes in the droplets width and length were measured and recorded over time (b). After 30 seconds the aqueous droplet started to boil (see change in transparency in a), which lead to strong emulsification of the sample. However, the droplet could not be forced out of the well.

The hybrid ITO-SD Chips were then used on the laser setup and a thermal bubble was induced near a well that contained sample droplets. A representative example of these studies is shown in Figure 29. After inducing a thermal bubble with the laser (red circle in image sequence of Figure 29a), the laser was actively moved in the image plane through the computer-user interface. The movement of the thermal bubble induced motion in the confined droplets and

forced the droplet out of the well. The change in droplet length and width (see Figure 29a) was recorded over time and is shown in Figure 29b. The nominal size of the well was 200 μm in length and 100 μm in width, representing the initial dimensions of the droplet. Within 10-15 seconds after inducing the thermal bubble, the droplet started to expand out of the well, thereby immediately filling the entire width of the main channel (150 μm). Now any further expansion was restricted to the length. After 20 seconds it was found that the sample droplet started to change in its transparency properties, indicating strong heating and subsequently bubbling of the aqueous sample. The growing thermal bubble was actively moved inside the well, thereby massaging the droplet out of the well. Despite the strong extension into the main channel and neighboring wells, the droplet could not be removed fully from the well. Instead the aqueous sample inside the well and close to the thermal bubble was increasingly heated, which lead to strong micro-emulsification as shown at 40 seconds (Figure 29a). The aqueous droplet and the thermally induced bubble remained in this condition, even after the laser was switched off. In addition, the thermal bubble remained in the well long after completion of the experiment. In a separate study a thermal bubble was created in bottom wells containing unconfined, spherical droplets that were on the order of 50 μm in diameter. In these studies it was found that the droplets could be moved around inside the bottom well. However, it was not possible to force the droplets into the narrow, 20 μm tall main channels. After 10-20 seconds the smaller sample droplets showed similar boiling characteristics as the larger droplet in Figure 29a. Additional studies were conducted to investigate the effect of prolonged thermal bubble growth. These studies resulted in a blow out of the samples through the main channel after prolonged heating.

3.2.4 Droplet Removal By Micropipetting

The droplet extraction by microneedles from bottom well SD Chips was successful for well sizes ranging from 2 nL to 16 nL. The main requirements for the method to succeed were *i)* a simple translational setup that holds the microneedle (Figure 30b) while providing control under a microscope (Figure 30a) and *ii)* the use of a thin PDMS membrane either as the bottom of microfluidic SD Chip containing the channel features or as the top containing the channel inlet/outlet ports (Figure 30c and d). The latter chip design requires multiple sealing steps to facilitate liquid inlet/outlet ports for fluid handling (*i* in Figure 30d). Using a chip design that combines channel structures and the thin membrane (Figure 30c) was found easier to fabricate and to handle for the micropipetting experiments.

Following sample self-digitization, the droplets could be easily accessed by the microneedle and it was possible to extract multiple droplets successively. Every injection site resealed itself after the needle was removed. The extraction of a 2 nL droplet is shown in brightfield images in Figure 31a. In a separate experiment a SD Chip with well sizes of 16 nL was used to compartmentalize a sample of mouse B-cells in culture media. The sample was supplemented with 25 μM Fluorescein to allow the visualization of the aqueous phase by fluorescence microscopy (Figure 31b). The overall control of fluid extraction was better in SD Chips with larger wells. The sample extraction by micropipetting was not complete with the simple setup used in this study. From the experiments shown in Figure 31 it can be seen that small fractions of the droplet remained in the wells after removal of the micropipette. It has to be noted that the pressure balancing during micropipetting and droplet removal was found to be challenging.

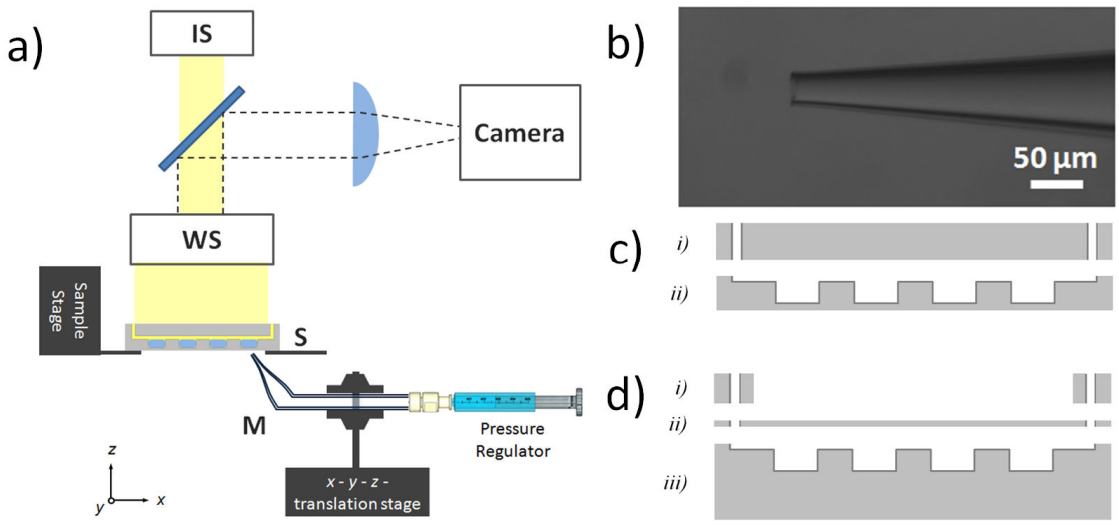

Figure 30. Sketch of the experimental setup used for targeted droplet removal (a). The microfluidic chip (S) and the tip of a micropipette (M) are visualized by a zoom scope. The scope has a wide area lens system (WS) and an illumination system (IS) for brightfield and fluorescence imaging. The micropipette is fixed in a 3-D micro-translation stage and connected to a pressure regulator to allow fluid extraction. b) Brightfield image of the tip from a pulled glass capillary used in this study. The chips for this study require a thin membrane that can be pierced by the capillary. The membrane can be either part of the PDMS cast (ii in c) or it can be part of the PDMS slab containing the inlet/outlet ports (ii in d). The design in (d) requires additional PDMS slabs with inlet/outlet port (i).

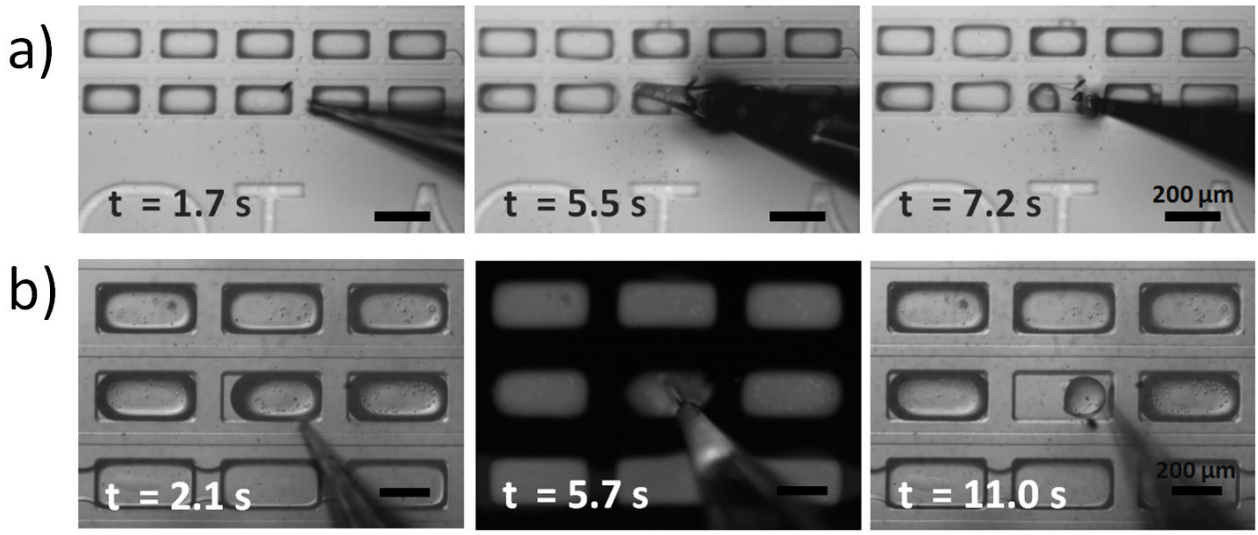

Figure 31. Sequences of brightfield and fluorescent microscopy images of aqueous droplet extraction from SD Chips with 2nL wells (a) and droplets containing mouse B-cells from SD Chips with 16 nL wells (b).

3.2.5 Conclusions

The four different methods tested for active droplet removal from the SD Chips had various challenges in the execution and, in part, required additional steps during the SD chip fabrication. Not all of the methods were successful in their intended tasks at the time these experiments were conducted. However, as the field of microfluidics is still developing, it can be expected that some of these methods will be valuable tools in the near future. A summary of all advantages and disadvantages of each method is given in Table 1.

The droplet removal by directly micropipetting the droplet out of the SD Chip proved to be the most successful and least destructive method. Droplets aspirated into the tip of a pulled glass capillary can be used for further studies by either directly dispensing the droplet onto a microscopic slide or by applying the capillary to other sample analysis methods (*e.g.*, nanoelectrospray mass spectrometry [113,116]). In addition, this method has a high potential for automatization of the micro-translation needle positioning and droplet extraction.

The other three non-invasive methods showed to have their own advantages and challenges for applications in SD Chips. The use of optical methods such as optical tweezers and taking advantage of thermocapillary flow showed little success despite the promises from current scientific literature. The methods were shown to work for droplets that are unconfined. The droplets in our SD Chips, however, are confined and despite being surrounded by an immiscible phase require large forces to be moved out of the wells. The forces that can be generated by these optical methods are on the order of nN [90]. Our mechanical studies with micropins showed that much larger forces are required to deform and move a droplet in the SD Chip than those generated by optical methods (*i.e.*, mN [99] versus nN [90]). One reason for this result may be

the strong adhesion of the droplet to the side walls of the wells as soon as it gets in contact with the substrate. Another method studied for indirect droplet interaction was the controlled generation of a convection bubble to drive the aqueous droplet out of the well. This method seemed feasible initially, but showed poor control over bubble growth and bubble movement within the channel. In addition, this method was partly destructive to the chip substrate (*i.e.*, burn marks at the PDMS-air interface outside the channel) and to the sample itself due to the large temperature gradient that is generated. Moreover, once the laser is switched off and the bubble growth stops, the poor heat dissipation prevents the generated bubble from disappearing.

Table 1. Summary of advantages and disadvantages of droplet removal methods.

Method	Pro's	Con's
Thermocapillary Flow/ Optical Tweezers	- Indirect sample interaction - precise control over force localization - non-destructive	- potential mixing with neighbouring droplets/wells - forces applied to the droplet are very small (~nN)
Mechanical Pin	- Indirect sample interaction - large forces can be applied - potential for automatization	- potential mixing with neighbouring droplets/wells - requires flexible substrates

Table 1 (continued). Summary of advantages and disadvantages of droplet removal methods.

Method	Pro's	Con's
Convection Bubble	- Indirect sample interaction - control over bubble localization	- potential mixing with neighbouring droplets/wells - bubbles are partly irreversible (slow heat dissipation) - limited control over bubble growth and direction - potential thermal sample destruction - requires more complex chip materials
Micropipetting	- good control over droplet extraction - droplets can be directly used in other methods - precise control over localization - potential for automatization	- Direct sample interaction - potential for cross-contamination - requires penetrable substrates - punctures/destroys the SD Chip

3.3 *Materials and Methods*

3.3.1 Microchip Fabrication

Microfluidic chips were fabricated by conventional soft lithography methods from SU-8 (MicroChem Corp., Newton, MA) similar to the procedures given in the previous chapter. The microfluidic structures were subsequently cast in PDMS (SYLGARD® 184 Silicone Elastomer Kit, Dow Corning, Corp., Midland, MI). Separately a flat PDMS slab for the inlets/outlets was cast on an featureless and silanized wafer. In the studies requiring thin membranes of feature layers, a small droplet of PDMS was placed on the feature master and allowed to spread, creating a thin layer (300-500 μm), before the PDMS was cured at 115°C. After the PDMS pieces were removed from the masters, inlet and outlet ports were cut into the featureless PDMS slab, the PDMS pieces were cleaned in with ethanol and blown dry with N_2 gas, and both pieces were placed inside of a plasma cleaner (Expanded Plasma Cleaner/Sterilizer; Harrick Plasma, Ithaca, NY). The plasma cleaner was evacuated thrice (< 100 mTorr) followed by purging with O_2. Finally, after the last purge with O_2 and following evacuation below 160 mTorr, the plasma was initiated at high level and left on for 45 seconds. The two PDMS pieces were brought in close contact immediately after removal from the plasma cleaner. Finally, the PDMS pieces were placed at 110-115°C for 24 hours to allow the PDMS convert back to its hydrophobic character.

For the thermal bubble studies a slightly modified procedure was used to make the chips. First, inlet and outlet ports were drilled into ITO slides (300 μm thick borosilicate glass, coating ITO 2800 ± 100 Å, resistivity 10 ± 2 ohms/sq; Thin Film Devices, Anaheim, CA). After cleaning the ITO slide with ethanol, PDMS slabs with cut out holes were sealed to one side of the slide

after brief alignment and following surface activation by oxygen plasma. Subsequently, the PDMS mould containing the channel structures was sealed to the opposite side of the ITO slide.

3.3.2 Sample Preparation

Different oils were used as *CP* in the experiments, including silicone oils (5 cSt, 50 cSt; Sigma Aldrich, Inc., St. Louis, MO) and mineral oil (30.0 cSt; light, embryo tested; Sigma Aldrich, Inc.). In order to facilitate droplet compartmentalization, the oils were supplemented with surfactants; Gransurf 77 (lot # 601497; Grant Industries, Inc., Elmwood Park, NJ) was used for silicone oils and Span 80 (Sorbiton monooleate, cat. #388912; Sigma Aldrich, Inc.) was used for the mineral oil at concentrations ranging from 0.01-1.00%$_{w/w}$.

Ultra-purified water (MilliQ; Millipore Corp., Billercia, MA) was used in all studies as *DP* except for those containing PCR mix or cells. The PCR mix was made from PCR buffer (Invitrogen Superscript 3) and supplemented with 0.05% Bovine Serum Albumin (BSA; Sigma Aldrich, Inc.). Samples with cells were based on dilutions of B-cell suspensions. The cells (mouse B lymphocyte 28-14-8S; cat. # HB-27^{TM}; ATCC, American Type Culture Collection, Manassas, VA) were cultured in RPMI-1640 (cat. #50-020-PC; Cellgro, Manassas, VA) supplemented with 10%$_{V/V}$ Fetal Bovine Serum (FBS; cat. # SH30071.03; Hyclone, Logan, UT) and 1%$_{V/V}$ Penicillin-Streptomycin (solubilized in citrate buffer; 10,000 units/ml penicillin, 10 mg/ml streptomycin; cat.# P4333; Sigma Aldrich, Inc.). Before the experiments, the B-cells were removed from the flasks facilitated by a cell scraper (Greiner Bio-One GmbH, Frickenhausen, GER), washed once in culture media (i.e., centrifugation at 450 g followed by decanting of the supernatant and resuspension in fresh media), and finally the cell concentration was evaluated

using a hemacytometer (AO Spencer Bright-Line, St. Louis, MO). Before the experiments the *DP* samples were supplemented with Fluorescein (10-100 μM; Reference Standard; cat. # F-1300; Molecular Probes, Invitrogen Corporation, Carlsbad, CA), in order to allow visualization of the *DP* by fluorescence microscopy.

3.3.3 Micropin and Micropipette Setup

Micropins were created from the blunted tips of hypodermic needles (30G; BD Bioscience, Bedford, MA). The needle tips were bent at an angle of 75° and the needle hub was connected to male fittings (Upchurch Scientific, Inc., Oak Harbor, WA). The needle fitting was then connected to a 3-dimensional translation stage (NRC / Newport Research Corp., Irvine, CA). The stage was fastened to a Multizoom Microscope (AZ100; Nikon Inc., Melville, NY; Figure 25).

Micropipettes were custom made from pulled glass capillaries and kindly provided by the Zhang Research Group at UW Chemistry. The glass capillaries had tips with approximately 30 μm outer diameter (Figure 30b). The tips were connected to a pressure regulator via PTFE tubing (20G, Zeus Industrial Products, Inc., Orangeburg, SC). The pressure regulator was based on a syringe (various sizes; BD Bioscience) connected to a custom made micromanipulator to provide control over syringe aspiration and dispensation. Similar to the micropin setup, the micropipette was fastened to fittings (Upchurch Scientific, Inc.), connected to a 3-dimensional translation stage (NRC / Newport Research Corp.), and fastened to a Multizoom Microscope (AZ100; Nikon Inc.; Figure 30a).

3.3.4 Optical Setup for Droplet Removal Studies

Two optical tweezers were built for the optical removal studies which are referred to as *i)* Setup 1 (single optical tweezers) and *ii)* Setup 2 (multi-optical tweezers). Both optical tweezers setups were based on a *4-f* system but differed in the type of laser used. Setup 1 was designed for a green light emitting frequency doubled Nd:YAG (neodymium-doped yttrium aluminum garnet; Nd:Y3Al5O12) Diode Pumped Solid State (DPSS) Laser Module with a wavelength of 532 nm (Model CW532-050; Roithner Laser Technik GmbH, Vienna, Austria). Setup 2 was built for a near IR laser (1064 nm, class 4; YLD-10LP; IPG Photonics Corp., Oxford, MA) and a spatial light modulator (SLM; HOLOEYE Photonics AG, Berlin, GER). The laser was first stirred by mirrors to facilitate alignment and subsequently expanded in both setups using a Keplarian telescope in order to fill the back aperture of the objective with 86% of a Gaussian beam (Figure 32). The objective was held in place by a custom built microscope in Setup 1 and in Setup 2 by an inverted microscope (Eclipse TE 2000-U; Nikon Inc., Melville, NY). In order to move the single foci created in Setup 1, the sample stage was adjusted by a precision *x*-*y*-*z*-micro-translation stage (). In Setup 2 the positioning of the laser foci was facilitated by a computer-user interface. The user interface was part of custom programmed software that is freely available from the University of Glasgow (http://www.physics.gla.ac.uk/Optics/).

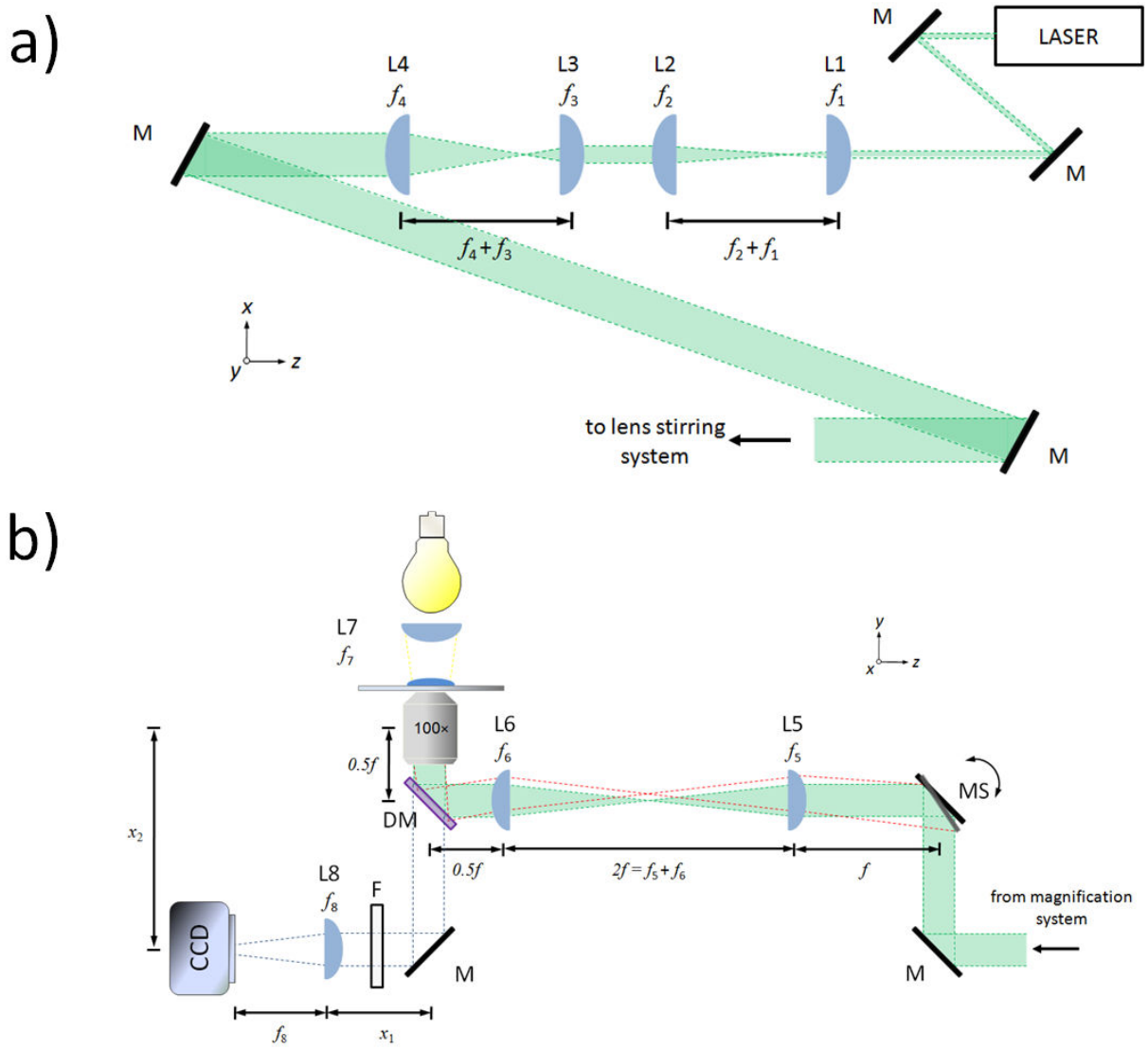

Figure 32. Schematic drawing of the optical lens system used in Setup 1 and 2. a) Lens system to expand the laser beam: the laser is stirred by mirrors (M) into two Keplarian telescopes (L1/L2 and L3/L4 and subsequently stirred into the lens stirring system (b). b) the laser is stirred into the back aperture of the objective by two mirrors, a 4f lens system (L5,L6), and a dichroic mirror (DM). The stirring mirror (MS) in Setup 2 is replaced by the SLM. The light of the illumination system is collected through the DM. A filter (F) is used to eliminate unwanted light and the image is projected into a camera by a tube lens (L8).

3.3.5 Image Acquisition and Data Analysis

Images were acquired using a CCD camera (GC 1380; Allied Vision Technologies Canada Inc., Burnaby, B.C., Canada) and custom coded image acquisition software (LabVIEW v8.6; National Instruments Corporation, Austin, TX).

CHAPTER 4

APPLICATIONS WITH BOTTOM WELL SELF-DIGITIZATION CHIPS

4 Applications with Bottom Well SD Chips

4.1 *Introduction and Background*

The bottom well SD Chip was shown in the previous chapters as a promising alternative to the SD design with side chambers. Self-Digitization in side chambers was shown to be a versatile method for next generation droplet platforms that take advantage of compartmentalizing a sample into thousands of nanoliter sized reactors. Self-digitization was presented in side chamber SD Chips as a suitable method for separating the crystal growth of otherwise concomitant polymorphs from a single solution [46]. By incorporating small changes in the fabrication of the devices, side chamber SD Chips were shown as promising platforms for point-of-care diagnostics, in particular when used for digital loop-mediated DNA amplification (dLAMP) [47]. Both applications, the crystal growth studies and the LAMP studies, rely on the compartmentalization of a sample into thousands of small nanoreactors. The predefined well size and the static array of nanodroplets then allowed the screening and quantification of individual samples within the nanodroplets.

Screening of individual samples is of great importance for every day diagnostics in the medical sciences. In particular the screening of blood samples for the presence of specific rare cells, such as circulating tumor cells, is a promising method for early disease state diagnostics. Many applications for rare cell screening rely on continuous flow methods and the ability to separate or sort target cells based on cell properties. These properties include size [117], fluorescence [118], and/or magnetism [119]. The inherent challenges with continuous flow methods lie in the addressability of samples containing rare cells after they are detected. To overcome these challenges, large arrays of wells have been used in the past for well seeding

studies by flooding the wells with aqueous cell suspension and relying on cell sedimentation to dock the cells in the wells [120]. Studies using this method showed successful time dependent live cell imaging [121,122] by screening of the well arrays. The docking of cells in wells by flooding a microwell chip with aqueous cell suspensions is a versatile method for prolonged cell studies. However, this method also has the potential of sample remixing as a result of limited cell docking. An improvement to these methods would be the use of an immiscible phase to create nanodroplets from cell suspensions directly in SD Chips and subsequently use the nano-droplet arrays as a rare event screening platform.

In order to investigate the feasibility of bottom well SD Chips as a rapid screening platform, we studied the sample self-compartmentalization from particle and cell suspensions. These suspensions were made from known concentrations of target and non-target specimen to mimic the concentration of a leukapheresis sample. Leukapheresis is a clinical cell separation procedure that is used to separate the white blood cells from whole blood. Leukapheresis samples are often used for research as a source of blood progenitor cells [123,124] and as a basis for autologous transplants in patients receiving high dose chemotherapy. The bottom well SD Chip is expected to be an improvement to existing screening methods for early disease state diagnostics with leukapheresis samples.

4.2 *Results and Discussion*

4.2.1 Sample Compartmentalization With Particle Suspensions

Suspensions that contain target specimen were compartmentalized in bottom well SD Chips (1,024 wells per chip, 2 nL wells). The entire chips were imaged under brightfield and fluorescence microscopy. Custom programmed software was subsequently used to screen through the images to detect target and non-target specimen in wells containing droplets. The data was then converted into color coded arrays that show the distribution of target and non-target specimen. An example distribution of non-target specimen in a 1,024 well chip is shown in Figure 33a, where the number of non-target specimen per well is shown as black (no specimen) and a temperature color scale from blue (1 specimen) to red (40 specimen). The distribution of target specimen is shown in a similar way, albeit limited to well position with respect to the array (Figure 33b).

A series of experiments was conducted to investigate the feasibility of the bottom well SD Chip for rare event screening. Chips with 1,024 wells were used and allowed the screening of sample suspensions with fractions of rare events ranging two orders of magnitude (*i.e.*, from 10^{-4} to 10^{-2}, Figure 33c). During the experiments it was found that the rare event detection was not dependent on the compartmentalization efficiency as long as the target cell fraction was large enough. The bottom well SD Chips used for the particle rare event studies had compartmentalization efficiencies of 81.2 ± 8.3% (n = 15). The overall trend in screening results followed the theoretical fraction closely (Figure 33c). The detection range can be further expanded to include lower target fractions by increasing the array size of the chips (*i.e.*, 10-fold increase to 10,024 wells).

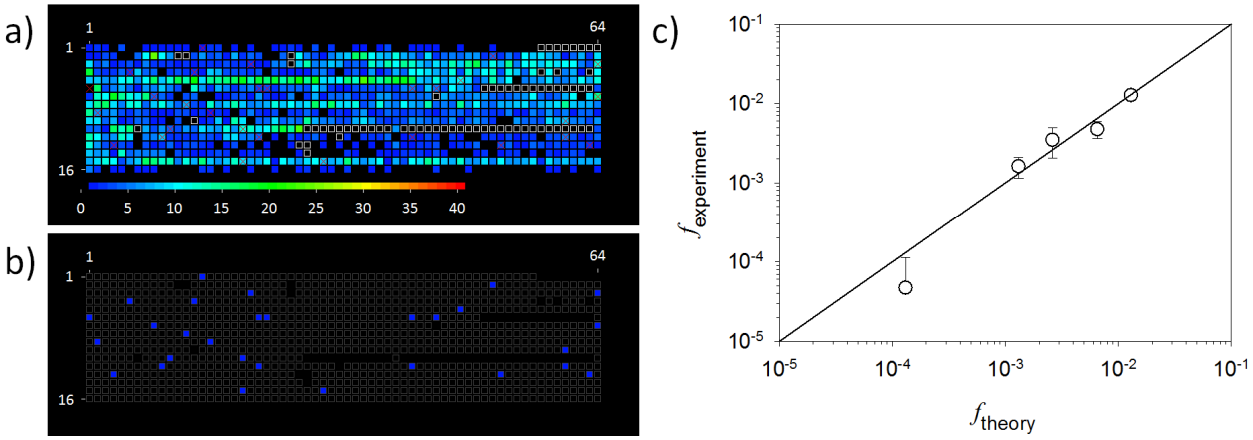

Figure 33. Results from rare event studies in bottom well SD Chips (1,024 wells per chip, 2 nL wells): a) Example of the distribution of non-target cells in the 16 × 64 well array shown in colour coding (no events = black, 40 cells per well = red). Wells without droplets are shown as white framed boxes. b) Distribution of target specimen (blue boxes) in the well array shown in (a). c) Comparison of expected and theoretical fractions of target specimen found in rare event screening studies with bottom well SD Chips. Data shown as mean ± SD (n=3).

The probability of non-target and target specimen per well can be estimated by taking the sample concentration per well into account ($C = cV_w$; c is the bulk concentration, V_w is the volume of a single well). The probability, p, to find a certain number of target particles, k, per well can be estimated by [125]:

$$p = \frac{(C)^k e^{-(C)}}{k!}$$

This equation was used to calculate the probability distribution for the 2 nL bottom well chips used in this study. For the mock sample concentration of 4.0×10^6 specimen/mL it was found

that there is a high probability for wells to have 7-8 non-target particles (black line Figure 34). As can be expected from the on-chip studies, the probability to find a well containing a target cell is low, and is approaching zero with decreasing target specimen fraction.

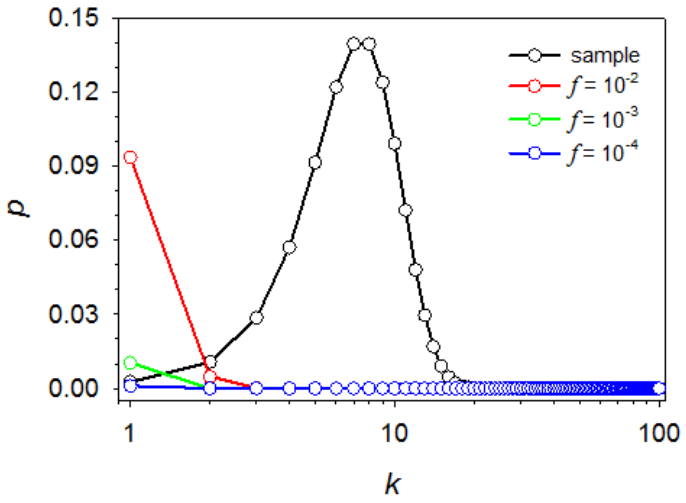

Figure 34. Probability of specimen per 2 nL well for sample concentration (black line) and selected target specimen fractions.

When the probability estimation is compared to the example shown in Figure 33a, it can be seen that the non-target cells are distributed across the chip with the majority of the wells showing well occupations between 1 and 15 specimen. This is within the expectation of the probability estimation shown in Figure 34. Furthermore, the distribution of target specimen in the wells appears to be random (Figure 33b). It has to be noted that the sample flow in this example is from left to right during sample compartmentalization.

4.2.2 Sample Compartmentalization With Cell Suspensions

The rare event studies were expanded to mock cell suspensions. Mouse B-cells were used to represent a leukapheresis sample. Immuno-fluorescently labeled cancer cells were spiked into the leukocyte sample at low concentrations. The sample was then used in a bottom well SD Chip that was scaled up from the chips used in the particle rare event studies. The scaled up bottom well SD Chip had 1,024 wells with an approximate volume of 16 nL per well. Extracting droplets with the micropipette setup from larger wells was found to be easier than from wells with a volume of 2 nL. The sample retention was high (*i.e.*, 99.7% in the example shown in Figure 35) with all wells containing single droplets with no interconnection to neighboring wells. The chip was then imaged by brightfield and fluorescence microscopy to identify the wells that contained the fluorescently labeled cancer cells (target cells). The fraction of target cells found from the image screening analysis (f_{Exp}) was 0.009, which was slightly higher than the theoretical concentration of target cells spiked into the sample (f_{theory} = 0.005). The deviation in spiked cell concentration from the nominal or theoretical concentration can be explained by the various processing steps required in cell experiments (*i.e.*, washing steps, pipetting, and bias in concentration evaluation). The cell number concentration was evaluated before mixing the two cell samples. Additional factors such as the formation of cell clusters which is not present in experiments with particles can contribute to variations in the actual cell concentration on chip. In addition, when compared to the screening experiments with fluorescent particles, the fluorescence intensity of target cells was found to be much lower and required careful imaging to avoid bleaching of the fluorescent labels (Figure 35d).

Subsequently, the micro-pipetting setup shown in the previous chapter was used to extract droplets from selected bottom wells of the SD Chip which contained target cells. The droplets extracted by micropipettes stayed in the micropipette tip and were ready for potential further applications. The droplets could either be dispensed carefully onto cover slides or sprayed out of the capillary by applying pressure to outlet of the capillary.

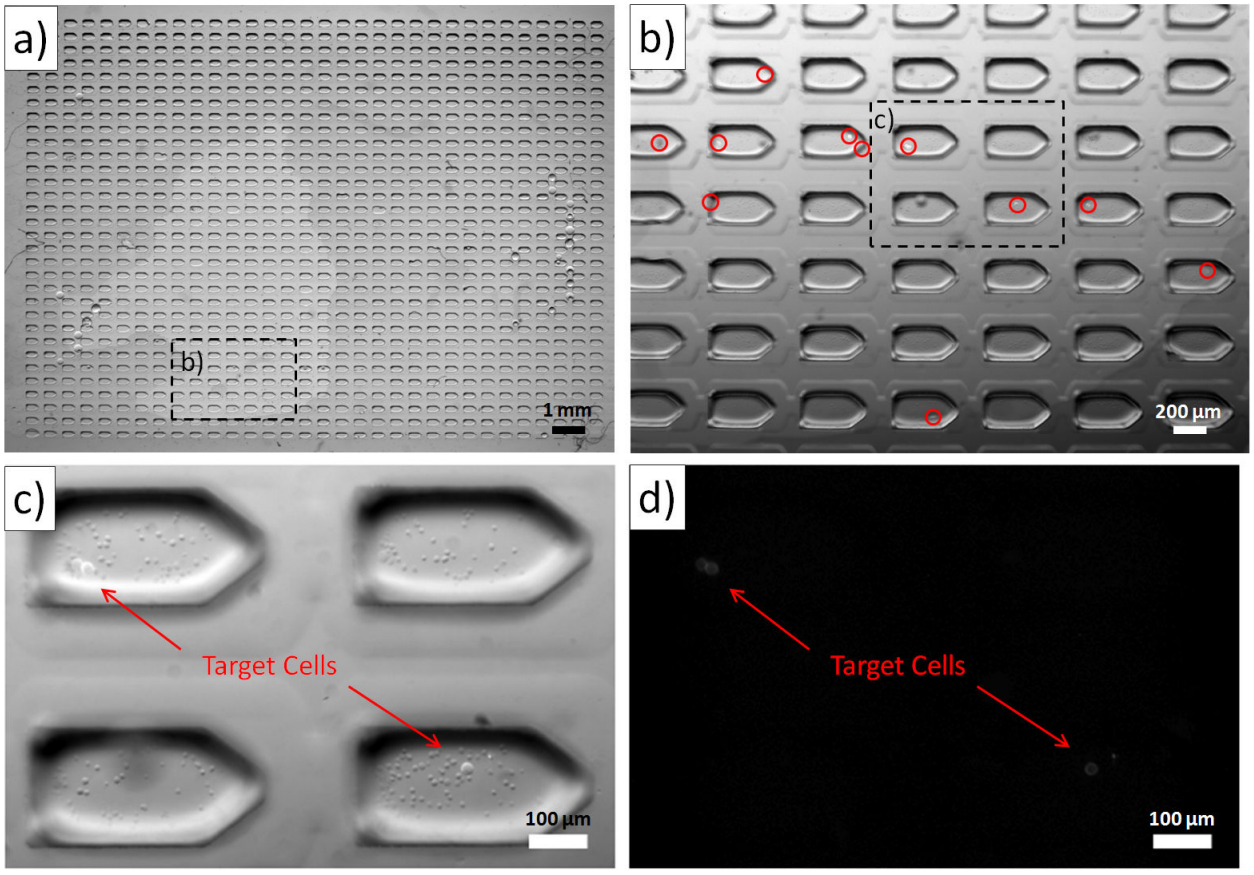

Figure 35. Rare cancer cell screening in bottom well SD Chips (1,024 wells per chip, 16 nL wells): The entire chip (a) is shown in brightfield with zoomed in sections (b). Red circles in (b) indicate positions of target cells obtained from analysis of high magnification images in brightfield and fluorescence (c, d).

Different potential applications are available to assay the (single) cells aspirated with the nano-droplet into the micropipette. These applications include single cell assays which either require additional cell culture or the direct analysis of the cells and the cell components by analytical methods (*e.g.*, Mass Spectrometry). At the current stage, the droplet compartmentalization in bottom well SD Chips was not conducted with a focus on sterile procedures which would allow the culture of extracted cells. Instead, the focus for extracted droplets was on the analysis by analytical methods. A flow chart of rare event screening followed by selective droplet extraction and the use of these potential applications is shown in (Figure 36). The two methods depicted in the Figure 36 which hold the greatest promise for single rare cell analysis are based on mass spectrometry and are Matrix-Assisted Laser Desorption/Ionization (MALDI) and Electrospray Ionization (ESI) methods. MALDI-MS has been recently shown to be a powerful tool to image individual cells and analyze the cell's protein composition [61-63]. Modern mass spectrometer combined with specialized cell preparation was required to allow the high resolution and sensitivity required to probe a single cancer cell [63]. This method represents the current state-of-the art for single cell analysis by MALDI-MS. (Nano-) Electrospray Ionization (ESI) is another ionization technique available for analysis of cell content by mass spectrometry [113,126]. In this ionization technique, a liquid sample is ionized by applying a large electric potential between the tip of a capillary and the vacuum inlet of the mass spectrometer. The sample is released as a mist of droplets following a charge build up at the capillary tip. The sample release occurs when the coulombic forces in the aqueous sample (induced by the electric charge of the capillary tip) exceed the surface tension of the solution (Rayleigh limit). The sample is then aspirated into the mass spectrometer by a combination of pressure and electrostatic potential difference.

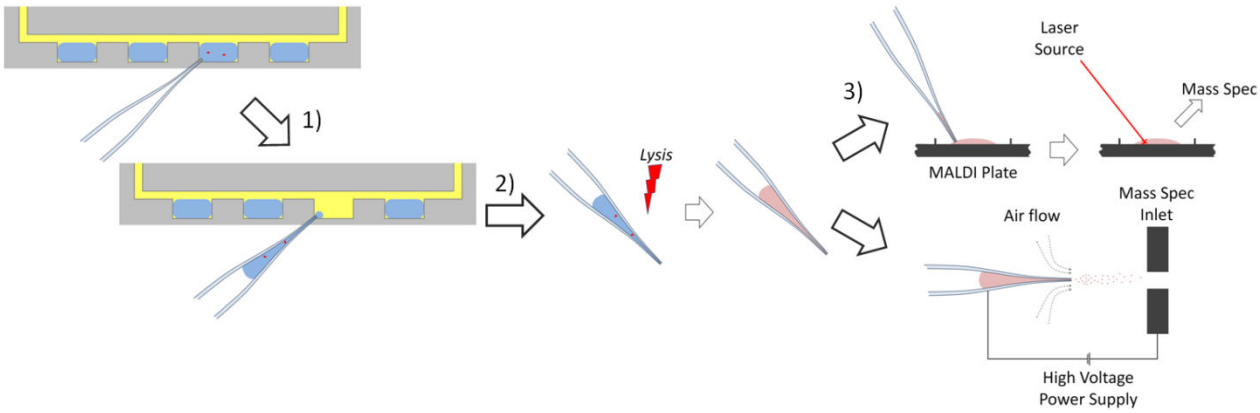

Figure 36. Nano-droplets with target cells extracted from bottom well SD Chips can be directly analyzed by mass spectrometry methods.

Preliminary studies showed that the equipment available for analysis of the extracted droplets will need additional modifications in order to allow the analysis of a single cell. The cell will need to be lysed inside the capillary by the use of either chemical gradients (*i.e.*, the use of ethanol/water mixtures), electrical lysis as part of the ESI (*i.e.*, creating large transmembrane gradients that result in membrane rupture), or the use of lasers for on-line cell lysis [127]. After cell lysis the sample will be analyzed by nano-ESI MS. All of these methods are based on the assumption that there is a distinguishable difference between the cell lines that can be detected by mass spectrometry using spectra fingerprinting.

In order to investigate the feasibility of nano-ESI MS several control experiments were conducted with sample containing only one cell type (*e.g.*, B-cells or cancer cells). The samples were prepared by dilution to obtain cell concentrations of 1 – 10 cells per nL (c = 1 – 10 × 10^6 cells/mL). Cell lysates from the samples with known cell concentration were then prepared by

resuspension in an ethanol/water mixture and analyzed by ESI-MS (using LCQ Deca ion trap mass spectrometer). Mass spectra were acquired over a mass range (m/z) of 300 – 2,000. The sample volume used to generate the mass spectra from the cell lysates corresponded to approximately 50 cells. Examples of two spectra from these studies are shown in Figure 37. From these mass spectra it can be seen that there is a visible difference between the two cell lines. In B cell line, different cell components can be detected in spectra that include mainly phospholipids (m/z = 700 - 900). The identification of phospholipids was confirmed by exact mass measurement using LTQ-Orbitrap mass spectrometer followed by a database search (LipidomicsGateway at LipidMaps.org). However, no tandem MS experiments were performed to further elucidate structure. In comparison, the spectra of the cancer cell line used in the study (SK-BR-3) were dominated by peaks in the region above m/z = 1400, which most likely corresponds to cytoplasmic proteins or peptides. Both cell samples were treated equally during preparation for mass spectrometry. The absence of phospholipids peaks in the region m/z = 700 - 900 in the spectra of the cancer cell line is most likely due to signal suppression (*i.e.*, competition for charge during ionization). The resolution of the ion trap mass spectrometer was not sufficient to resolve the individual multiple charged proteins in the spectra region above m/z = 1400. The presence of these proteins in the cancer cell samples but not in the B-cell samples could be explained with the fast metabolism of cancer cells.

The cell lysate studies presented here provide a foundation to develop a data base for spectra fingerprinting. Further studies will be required to define distinct differences between various cell types. The number of cells required to acquire spectra with good resolution was between 50 and 100. As a result, no spectra were acquired from the 2 nL droplets extracted from the bottom well SD chips by micropipetting.

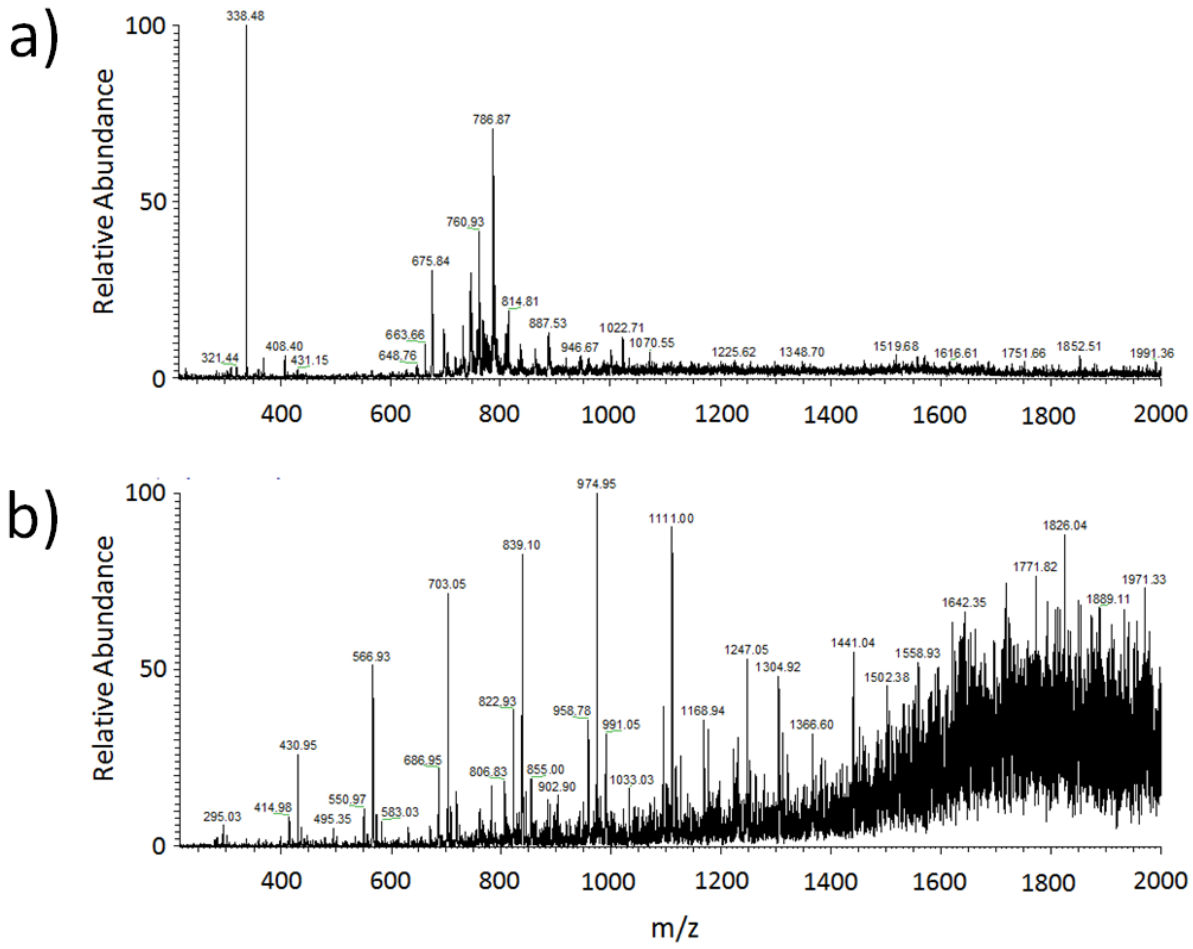

Figure 37. Mass spectra from ESI MS of cell lysates samples containing a) mouse B-lymphocytes and b) human epithelial breast carcinoma cell (SK-BR-3).

4.3 *Conclusions*

The bottom well SD Chip has been shown to be a potential next generation droplet platform for use as a rare event screening method. Studies with mock samples of fluorescent particles have been used to show a dynamic range for detecting rare specimen across two orders of magnitude in a bottom well SD Chip with 1,024 wells. The measured rare event fraction corresponded well with the theoretical rare event fraction and ranged from 1 in 100 to close to 1 in 10,000 (rare cells in non-target cells). A scale up of the bottom well SD Chips to arrays with 10,000 to 100,000 wells is expected to increase the dynamic range. A larger dynamic detection range will allow the detection of rare cells (*e.g.*, rare CTCs or hematopoietic stem cells in bone marrow samples [119]) and the use of the bottom well SD Chip as a rare cell screening platform will provide the foundation for analytical assays that can be conducted with these rare cells. An example of such analytical assay was shown with ESI-MS. The initial studies presented here were conducted with cell lysates of 50-100 cells per mass spectra and were limited by the detection limits of the mass spectrometer. Further improvements of the analysis protocol will allow the direct coupling of rare even screening in bottom well SD Chips, cell extraction by micro-pipetting, and subsequent analysis of single cells by nano-ESI-MS. A comparison of the mass spectra acquired from the single cell can then be compared to a data base of markers obtained from bulk samples.

4.4 *Materials and Methods*

4.4.1 Microchip Fabrication

Similar to the procedures given in the previous chapters, microfluidic chips were fabricated by conventional soft lithography methods from negative epoxy-type photoresist (SU-8; MicroChem Corp.), cast from PDMS (SYLGARD® 184 Silicone Elastomer Kit, Dow Corning, Corp.), and sealed by oxygen plasma. The chips were subsequently kept at 110-115°C for at least 24 hours to allow the PDMS convert back to its hydrophobic character.

4.4.2 Sample Preparation

Silicone oil (5 and 50 cSt; Sigma Aldrich, Inc., St. Louis, MO) and mineral oil (30.0 cSt; light, embryo tested; Sigma Aldrich, Inc.) was used as *CP*. In order to facilitate droplet compartmentalization, the oils were supplemented with surfactants; Gransurf 77 (lot # 601497; Grant Industries, Inc., Elmwood Park, NJ) was used for silicone oils and Span 80 (Sorbiton monooleate, cat. #388912; Sigma Aldrich, Inc.) was used for the mineral oil at concentrations ranging of $0.01\%_{w/w}$ and $0.02\%_{w/w}$, respectively. Particle and cell suspensions of known concentrations were used as *DP*. Stock solutions of target and non-target specimen were prepared based on concentration evaluation by a hemacytometer (AO Spencer Bright-Line, St. Louis, MO).

Different fluorescent and non-fluorescent particles were used for the rare event studies with particles. Green fluorescent particles (9.9 μm; cat. # G1000; Duke Scientific Corp., Palo Alto, CA) were used as non-target specimen. Red fluorescent particles (15 μm; cat. # 36-4; Duke

Scientific) were used as target specimen. The particles were subsequently diluted in ultra-pure water (MilliQ) and mixed to obtain specific ratios of target to non-target particles.

Cell samples for the rare event studies were made from mouse B-cells, representing the non-target leukocyte fraction, and a human epithelial breast carcinoma cell line (SK-BR-3), representing the target cancer cells. The mouse B-cells (mouse B lymphocyte; cat. # HB-27TM; ATCC, American Type Culture Collection, Manassas, VA, USA) were cultured in RPMI-1640 (cat. #50-020-PC; Cellgro, Manassas, VA) and the human epithelial breast carcinoma cells (SK-BR-3; cat. # HTB-30TM; ATCC) were cultured in McCoy's 5A Medium (cat. # 30-2007; ATCC). All culture media were supplemented with $10\%_{V/V}$ Fetal Bovine Serum (FBS; cat. # SH30071.03; Hyclone, Logan, UT) and $1\%_{V/V}$ Penicillin-Streptomycin (solubilized in citrate buffer; 10,000 units/ml penicillin, 10 mg/ml streptomycin; cat.# P4333; Sigma Aldrich, Inc., St. Louis, MO, USA). The cells were cultured according to protocols provided by the ATCC at 37°C and 5% CO_2.

Before the experiments, the B-cells and SK-BR-3 cells were removed from the flasks facilitated by a cell scraper (Greiner Bio-One GmbH, Frickenhausen, GER). Each cell line was washed once in labeling buffer (1× phosphate buffered saline (PBS), 2 mM Ethylenediaminetetraacetic acid (EDTA; cat. no. E9884; Sigma Aldrich, Inc.), 0.5% Bovine Serum Albumin (BSA; cat. no. A3059; Sigma Aldrich, Inc.), and resuspended in labeling buffer. Finally, the cell concentration was evaluated using a hemacytometer (AO Spencer Bright-Line). The B-cell sample was adjusted to 5.0×10^6 cells/mL and stored at 4°C, while from the SK-BR-3 cell sample 1.0×10^6 cells were aliquoted and pelleted. The SK-BR-3 pellet was subsequently labeled with fluorescent antibodies (20 μL per 10^6 cells, anti-EpCAM-PE; cat.# 324206; BioLegend, San Diego, CA),

incubated in dark at 4°C for 30 min, washed once in labeling buffer, and after resuspension subjected to cell concentration evaluation. The labeled SK-BR-3 cells were then diluted and spiked into the B-cell sample to obtain a sample concentration of 4.0×10^6 cells/mL with ratios of target to non-target cells between 1:20 to 1:20,000.

4.4.3 Experimental Procedure for Rare Event Screening

All experiments were conducted with a pre-filled segmented plug (oil – sample - oil) in the inlet tubing as noted in the previous chapters. Droplet compartmentalization was conducted immediately after the plugs were segmented in the tubing, in order to minimize particle sedimentation. The chips were subsequently imaged under a wide area microscopy (AZ100 Multizoom; Nikon Inc., Melville, NY; Zoom Stereo Microscope SZ61; Olympus Imaging America Inc.; Center Valley, PA) at high magnification. Images were acquired by scanning manually across the chip and taking images from overlapping arrays of wells under brightfield, and under two fluorescence settings to capture the fluorescence of particles or cells. Images were acquired with a high-resolution CCD camera (GC 1380; Allied Vision Technologies Canada Inc., Burnaby, B.C., Canada) and a custom coded LabVIEW software (v8.6; National Instruments Corporation, Austin, TX)

The images of each experiment were subsequently analyzed by custom programmed software (LabVIEW), which compared the brightfield and fluorescent images and allowed the enumeration of target particles per microfluidic chip. All images were subsequently checked manually to evaluate the accuracy of the program. Finally, the micro-pipetting setup was used to

extract selected droplets, following detection of target specimen in the compartmentalized droplets.

4.4.4 Cell Analysis By Mass Spectrometry

Samples for analysis by mass spectrometry were prepared similar to the samples used for the rare event studies in bottom well SD Chips. The cell sample concentration was adjusted by dilution from a stock sample after concentration analysis using a hemacytometer (AO Spencer Bright-Line). The cells were subsequently washed twice in ultra-pure water (MilliQ). Cell lysis was achieved by dispersion of the cell pellet in a 1:1 solution of ethanol ultra-pure water. The mass spectra were obtained using a LCQ-Deca ion trap mass spectrometer (ThermoFisher Scientific; formerly Thermo Electron) using electrospray ionization.

5 List of References

[1] Gravesen P, Branebjerg J, Jensen OJ (1993). *Microfluidics - A review*. J Micromech Microeng **3**, 168-182.

[2] Xia Y, Whitesides GM (1998). *Soft lithography*. Annu Rev Mater Sci **28**, 153–184.

[3] Mukhopadhyay R (2009). *Microfluidics: on the slope of enlightenment*. Anal Chem **81**, 4169-73.

[4] Mukhopadhyay R (2006). *Diving into droplets*. Anal Chem **78**, 1401-4.

[5] Pamme N (2006). *Magnetism and microfluidics*. Lab Chip **6**, 24-38.

[6] Di Carlo D (2009). *Inertial microfluidics*. Lab Chip **9**, 3038-46.

[7] Cho SH, Godin JM, et al. (2010). *Review Article: Recent advancements in optofluidic flow cytometer*. Biomicrofluidics **4**, 043001.

[8] Martinez AW, Phillips ST, et al. (2010). *Diagnostics for the developing world: microfluidic paper-based analytical devices*. Anal Chem **82**, 3-10.

[9] Kuo JS, Chiu DT (2011). *Controlling mass transport in microfluidic devices*. Annu Rev Anal Chem (Palo Alto Calif) **4**, 275-96.

[10] Friend J, Yeo LY (2011). *Microscale acoustofluidics: Microfluidics driven via acoustics and ultrasonics*. Rev Mod Phys **83**, 647–704.

[11] Choi K, Ng AH, et al. (2012). *Digital microfluidics*. Annu Rev Anal Chem (Palo Alto Calif) **5**, 413-40.

[12] Garstecki P, Fuerstman MJ, et al. (2006). *Formation of droplets and bubbles in a microfluidic T-junction-scaling and mechanism of break-up*. Lab Chip **6**, 437-46.

[13] Anna SL, Bontoux N, Stone HA (2003). *Formation of dispersions using "flow focusing" in microchannels*. Applied Physics Letters **82**, 364-366

[14] Haeberle S, Zengerle R, Ducree J (2007). *Centrifugal generation and manipulation of droplet emulsions*. Microfluidic Nanofluidic **3**, 65-75.

[15] Song H, Tice JD, Ismagilov RF (2003). *A microfluidic system for controlling reaction networks in time*. Angew Chem Int Ed Engl **42**, 768-72.

[16] Skelley AM, Kirak O, et al. (2009). *Microfluidic control of cell pairing and fusion*. Nat Methods **6**, 147-52.

[17] Baroud CN, Gallaire F, Dangla R (2010). *Dynamics of microfluidic droplets*. Lab Chip **10**, 2032-45.

[18] Sgro AE, Allen PB, Chiu DT (2007). *Thermoelectric manipulation of aqueous droplets in microfluidic devices*. Anal Chem **79**, 4845-51.

[19] Lee H, Kim J, et al. (2010). *Colour-barcoded magnetic microparticles for multiplexed bioassays*. Nat Mater **9**, 745-9.

[20] Anna SL, Mayer HC (2006). *Microscale tipstreaming in a microfluidic flow focusing device*. Physics of Fluids **16**, 121512.

[21] He M, Kuo JS, Chiu DT (2005). *Electro-generation of single femtoliter and picoliter-volume aqueous droplets in microfluidic systems*. Applied Physical Letters **87**, 031916

[22] Lorenz RM, Edgar JS, et al. (2006). *Microfluidic and optical systems for the on-demand generation and manipulation of single femtoliter-volume aqueous droplets*. Anal Chem **78**, 6433-9.

[23] Chiu DT, Lorenz RM (2009). *Chemistry and biology in femtoliter and picoliter volume droplets*. Acc Chem Res **42**, 649-58.

[24] He M, Edgar JS, et al. (2005). *Selective encapsulation of single cells and subcellular organelles into picoliter- and femtoliter-volume droplets*. Anal Chem **77**, 1539-44.

[25] Lorenz RM, Fiorini GS, et al. (2008). *Simultaneous generation of multiple aqueous droplets in a microfluidic device*. Anal Chim Acta **630**, 124-30.

[26] Jeffries GD, Edgar JS, et al. (2007). *Using polarization-shaped optical vortex traps for single-cell nanosurgery*. Nano Lett **7**, 415-20.

[27] Zeigler MB, Chiu DT (2009). *Laser selection significantly affects cell viability following single-cell nanosurgery*. Photochem Photobiol **85**, 1218-24.

[28] Tice JD, Lyon AD, Ismagilov RF (2004). *Effects of viscosity on droplet formation and mixing in microfluidic channels*. Anal Chim Acta **507**, 73-77.

[29] Nie Z, Xu S, et al. (2005). *Polymer particles with various shapes and morphologies produced in continuous microfluidic reactors*. J Am Chem Soc **127**, 8058-63.

[30] Di Carlo D, Aghdam N, Lee LP (2006). *Single-cell enzyme concentrations, kinetics, and inhibition analysis using high-density hydrodynamic cell isolation arrays*. Anal Chem **78**, 4925-30.

[31] Di Carlo D, Wu LY, Lee LP (2006). *Dynamic single cell culture array*. Lab Chip **6**, 1445-9.

[32] Lau BT, Baitz CA, et al. (2007). *A complete microfluidic screening platform for rational protein crystallization*. J Am Chem Soc **129**, 454-5.

[33] Shi W, Qin J, et al. (2008). *Droplet-based microfluidic system for individual Caenorhabditis elegans assay*. Lab Chip **8**, 1432-5.

[34] Huebner A, Bratton D, et al. (2009). *Static microdroplet arrays: a microfluidic device for droplet trapping, incubation and release for enzymatic and cell-based assays*. Lab Chip **9**, 692-8.

[35] Edgar JS, Milne G, et al. (2009). *Compartmentalization of chemically separated components into droplets*. Angew Chem Int Ed Engl **48**, 2719-22.

[36] Bithi SS, Vanapalli SA (2010). *Behavior of a train of droplets in a fluidic network with hydrodynamic traps*. Biomicrofluidics **4**, 044110-1.

[37] Shim JU, Cristobal G, et al. (2007). *Control and measurement of the phase behavior of aqueous solutions using microfluidics*. J Am Chem Soc **129**, 8825-35.

[38] Shim JU, Olguin LF, et al. (2009). *Simultaneous determination of gene expression and enzymatic activity in individual bacterial cells in microdroplet compartments*. J Am Chem Soc **131**, 15251-6.

[39] Schmitz CHJ, Rowat AC, et al. (2009). *Dropspots: a picoliter array in a microfluidic device*. Lab on a Chip **9**, 44-49.

[40] Hatch AC, Fisher JS, et al. (2011). *Tunable 3D droplet self-assembly for ultra-high-density digital micro-reactor arrays*. Lab Chip **11**, 2509-17.

[41] Hatch AC, Fisher JS, et al. (2011). *1-Million droplet array with wide-field fluorescence imaging for digital PCR*. Lab Chip **11**, 3838-45.

[42] Heyries KA, Tropini C, et al. (2011). *Megapixel digital PCR*. Nat Methods **8**, 649-51.

[43] Sundberg SO, Wittwer CT, et al. (2010). *Spinning disk platform for microfluidic digital polymerase chain reaction*. Anal Chem **82**, 1546-50.

[44] Du W, Li L, et al. (2009). *SlipChip*. Lab Chip **9**, 2286-92.

[45] Li L, Du W, Ismagilov R (2010). *User-loaded SlipChip for equipment-free multiplexed nanoliter-scale experiments*. J Am Chem Soc **132**, 106-11.

[46] Cohen DE, Schneider T, et al. (2010). *Self-Digitization of Sample Volumes*. Analytical Chemistry **82**, 5707–5717.

[47] Gansen A, Herrick AM, et al. (2012). *Digital LAMP in a sample self-digitization (SD) chip*. Lab Chip **12**, 2247-54.

[48] Vogelstein B, Kinzler KW (1999). *Digital PCR*. Proc Natl Acad Sci U S A **96**, 9236-41.

[49] Baker M (2010). *Clever PCR: more genotyping, smaller volumes*. Nature **7**, 351-356.

[50] Devonshire AS, Sanders R, et al. (2012). *Application of next generation qPCR and sequencing platforms to mRNA biomarker analysis*. Methods **in press (dx.doi.org/10.1016/j.ymeth.2012.07.021)**

[51] Pinheiro LB, Coleman VA, et al. (2012). *Evaluation of a droplet digital polymerase chain reaction format for DNA copy number quantification*. Anal Chem **84**, 1003-11.

[52] Zeng Y, Novak R, et al. (2010). *High-performance single cell genetic analysis using microfluidic emulsion generator arrays*. Anal Chem **82**, 3183-90.

[53] Shen F, Du W, et al. (2010). *Nanoliter Multiplex PCR Arrays on a SlipChip*. Analytical Chemistry **82**, 4606–4612.

[54] Shen F, Sun B, et al. (2011). *Multiplexed quantification of nucleic acids with large dynamic range using multivolume digital RT-PCR on a rotational SlipChip tested with HIV and hepatitis C viral load*. J Am Chem Soc **133**, 17705-12.

[55] Shen F, Davydova EK, et al. (2011). *Digital Isothermal Quantification of Nucleic Acids via Simultaneous Chemical Initiation of Recombinase Polymerase Amplification Reactions on SlipChip*. Analytical Chemistry **DOI: 10.1021/ac200247e**

[56] Kelly RT, Page JS, et al. (2009). *Dilution-free analysis from picoliter droplets by nano-electrospray ionization mass spectrometry*. Angew Chem Int Ed Engl **48**, 6832-5.

[57] Kelly RT, Tang K, et al. (2008). *Elastomeric microchip electrospray emitter for stable cone-jet mode operation in the nanoflow regime*. Anal Chem **80**, 3824-31.

[58] Ji J, Nie L, et al. (2012). *Proteolysis in microfluidic droplets: an approach to interface protein separation and peptide mass spectrometry*. Lab Chip **12**, 2625-9.

[59] Sun S, Slaney TR, Kennedy RT (2012). *Label free screening of enzyme inhibitors at femtomole scale using segmented flow electrospray ionization mass spectrometry*. Anal Chem **84**, 5794-800.

[60] Baker CA, Roper MG (2012). *Online coupling of digital microfluidic devices with mass spectrometry detection using an eductor with electrospray ionization*. Anal Chem **84**, 2955-60.

[61] Amantonico A, Urban PL, et al. (2010). *Single-cell MALDI-MS as an analytical tool for studying intrapopulation metabolic heterogeneity of unicellular organisms*. Anal Chem **82**, 7394-400.

[62] Lanni EJ, Rubakhin SS, Sweedler JV (2012). *Mass spectrometry imaging and profiling of single cells*. J Proteomics **75**, 5036-51.

[63] Schober Y, Guenther S, et al. (2012). *Single cell matrix-assisted laser desorption/ionization mass spectrometry imaging*. Anal Chem **84**, 6293-7.

[64] Courtois F, Olguin LF, et al. (2008). *An integrated device for monitoring time-dependent in vitro expression from single genes in picolitre droplets*. Chembiochem **9**, 439-46.

[65] Brouzes E, Medkova M, et al. (2009). *Droplet microfluidic technology for single-cell high-throughput screening*. Proc Natl Acad Sci U S A **106**, 14195-200.

[66] El Debs B, Utharala R, et al. (2012). *Functional single-cell hybridoma screening using droplet-based microfluidics*. Proc Natl Acad Sci U S A **109**, 11570-5.

[67] Li L, Du W, Ismagilov RF (2010). *Multiparameter screening on SlipChip used for nanoliter protein crystallization combining free interface diffusion and microbatch methods*. J Am Chem Soc **132**, 112-9.

[68] Venancio-Marques A, Liu Y-J, et al. (2012). *Modification-Free Photocontrol of β-Lactam Conversion with Spatiotemporal Resolution*. ACS Synthetic Biology **dx.doi.org/10.1021/sb300010a |**

[69] Fallah-Araghi A, Baret JC, et al. (2012). *A completely in vitro ultrahigh-throughput droplet-based microfluidic screening system for protein engineering and directed evolution*. Lab Chip **12**, 882-91.

[70] Matosevic S, Paegel BM (2011). *Stepwise synthesis of giant unilamellar vesicles on a microfluidic assembly line*. J Am Chem Soc **133**, 2798-800.

[71] Gañan-Calvo AM, Martin-Banderas L, et al. (2006). *Straightforward production of encoded microbeads by Flow Focusing: Potential applications for biomolecule detection*. Int J Pharm **324**, 19-26.

[72] Häfeli UO, Saatchi K, et al. (2010). *Lung Perfusion Imaging with Monosized Biodegradable Microspheres*. Biomacromolecules **11**, 561–567.

[73] Teh SY, Lin R, et al. (2008). *Droplet microfluidics*. Lab Chip **8**, 198-220.

[74] Chiu DT (2010). *Interfacing droplet microfluidics with chemical separation for cellular analysis* Analytical and Bioanalytical Chemistry **397**, 1618-2642.

[75] Theberge AB, Courtois F, et al. (2010). *Microdroplets in microfluidics: an evolving platform for discoveries in chemistry and biology*. Angew Chem Int Ed Engl **49**, 5846-68.

[76] Pompano RR, Liu W, et al. (2011). *Microfluidics Using Spatially Defined Arrays of Droplets in One, Two, and Three Dimensions*. Annu Rev Anal Chem **4**, 59–81.

[77] Abate AR, Poitzsch A, et al. (2009). *Impact of inlet channel geometry on microfluidic drop formation*. Physical Review E **80**, 026310.

[78] Donzel C, Geissler M, et al. (2001). *Hydrophilic Poly(dimethylsiloxane) Stamps for Microcontact Printing*. Advanced materials **13**, 1164–1167.

[79] Jin M, Feng X, et al. (2005). *Super-Hydrophobic PDMS Surface with Ultra-Low Adhesive Force*. Macromolecular Rapid Communications **26**, 1805-1809.

[80] Kintses B, van Vliet LD, et al. (2010). *Microfluidic droplets: new integrated workflows for biological experiments*. Curr Opin Chem Biol **14**, 548-55.

[81] Burnham DR, Schneider T, Chiu DT (2010). *Optical trapping enabled parallel delivery of biological stimuli with high spatial and temporal resolution*. Proceedings of the International Society for Optical Engineering **7762**, 77621T.

[82] Song JW, Gu W, et al. (2005). *Computer-controlled microcirculatory support system for endothelial cell culture and shearing*. Anal Chem **77**, 3993-9.

[83] Yen GS, Fujimoto BS, et al. (2010). *A Rapid and Economical Method for Profiling Feature Heights during Microfabrication*. Lab on a Chip **11**, 974-977.

[84] Klinger T (2003). *Image processing with LabVIEW and IMAQ vision*. Prentice Hall PTR, Upper Saddle River, NJ.

[85] Ashkin A, Dziedzic JM, et al. (1986). *Observation of a single-beam gradient force optical trap for dielectric particles*. Opt Lett **11**, 288.

[86] McGloin D (2006). *Optical tweezers: 20 years on*. Philos Transact A Math Phys Eng Sci **364**, 3521-37.

[87] Marangoni C (1871). *Ueber die Ausbreitung der Tropfen einer Flüssigkeit auf der Oberfläche einer anderen*. Annalen der Physik **219**, 337-354.

[88] Plateau J, Lanza MC (1880). *On the Superficial Viscidity of Liquids*. Science **1**, 298-302.

[89] Young NO, Goldstein JS, Block MJ (1959). *The motion of bubbles in a vertical temperature gradient*. Journal of Fluid Mechanics **6**, 350-356.

[90] Verneuil E, Cordero M, et al. (2009). *Laser-induced force on a microfluidic drop: origin and magnitude*. Langmuir **25**, 5127-34.

[91] Baroud CN, Delville J-P, et al. (2007). *Thermocapillary valve for droplet production and sorting*. Physical Review E **75**, 046302.

[92] Vincent MRdS, Wunenburger R, Delville J-P (2008). *Laser switching and sorting for high speed digital microfluidics* Applied Physics Letters **92**, 154105.

[93] Weaver JA, Melin J, et al. (2010). *Static control logic for microfluidic devices using pressure-gain valves*. Nature Physics **6**, 218 - 223.

[94] Fordyce PM, Gerber D, et al. (2010). *De novo identification and biophysical characterization of transcription-factor binding sites with microfluidic affinity analysis*. Nat Biotechnol **28**, 970-5.

[95] Maerkl SJ, Quake SR (2007). *A systems approach to measuring the binding energy landscapes of transcription factors*. Science **315**, 233-7.

[96] Doh I, Cho YH (2009). *Passive flow-rate regulators using pressure-dependent autonomous deflection of parallel membrane valves*. Lab Chip **9**, 2070-5.

[97] Hartono D, Liu Y, et al. (2011). *On-chip measurements of cell compressibility via acoustic radiation*. Lab Chip **11**, 4072-4080.

[98] Rho JY, Ashman RB, Turner CH (1993). *Young's modulus of trabecular and cortical bone material: ultrasonic and microtensile measurements*. J Biomech **26**, 111-9.

[99] Gu W, Zhu X, et al. (2004). *Computerized microfluidic cell culture using elastomeric channels and Braille displays*. Proc Natl Acad Sci U S A **101**, 15861-6.

[100] Heo YS, Cabrera LM, et al. (2012). *Real time culture and analysis of embryo metabolism using a microfluidic device with deformation based actuation*. Lab Chip **12**, 2240-6.

[101] Betz AR, Xu J, et al. (2010). *Do surfaces with mixed hydrophilic and hydrophobic areas enhance pool boiling?* Applied Physics Letters **97**

[102] Zhang K, Jian A, et al. (2011). *Laser-induced thermal bubbles for microfluidic applications*. Lab Chip **11**, 1389-95.

[103] Ohl C-D, Arora M, et al. (2006). *Surface cleaning from laser-induced cavitation bubbles* Applied Physics Letters **89**, 074102.

[104] Zwaan E, Le Gac S, et al. (2007). *Controlled cavitation in microfluidic systems*. Phys Rev Lett **98**, 254501.

[105] Sun K, Yamaguchi A, et al. (2002). *A heater-integrated transparent microchannel chip for continuous-flow PCR*. Sensors and Actuators B: Chemical **84**, 283-289.

[106] Amaral A, De Carvalho CN, et al. (2005). *ITO properties on anisotropic flexible transparent cellulosic substrates under different stress conditions*. Materials Science and Engineering B **118**, 183-186.

[107] Kim DH, Park MR, et al. (2006). *Thickness dependence of electrical properties of ITO film deposited on a plastic substrate by RF magnetron sputtering*. Applied Surface Science **253**, 409-411.

[108] Willis DA, Dreier AL (2009). *Laser micromachining of indium tin oxide films on polymer substrates by laser-induced delamination*. Journal of Physics D: Applied Physics **42**, 045306 (8pp).

[109] Pasteur M (1884). *Louis Pasteur*. Science **3**, 546-9.

[110] Reyniers JA (1932). *A New and Simplified Micrurgical Apparatus Especially Adapted to Single Cell Isolation*. J Bacteriol **23**, 183-192.

[111] Hochmuth RM (2000). *Micropipette aspiration of living cells*. J Biomech **33**, 15-22.

[112] Jarrell JA, King JG, Mills JW (1981). *A scanning micropipette molecule microscope*. Science **211**, 277-9.

[113] Wilm M, Mann M (1996). *Analytical properties of the nanoelectrospray ion source*. Anal Chem **68**, 1-8.

[114] Burnham DR, Schneider T, Chiu DT (2011). *Effects of aliasing on the fidelity of a two dimensional array of foci generated with a kinoform*. Optics Express **19**, 17121-17126.

[115] Martino M, Luches A, et al. (2001). *Characterization of thin indium tin oxide films deposited by pulsed XeCl laser ablation*. Journal of Physics D: Applied Physics **34**, 2606–2609.

[116] Mao P, Wang HT, et al. (2011). *Multinozzle emitter arrays for nanoelectrospray mass spectrometry*. Anal Chem **83**, 6082-9.

[117] Sethu P, Sin A, Toner M (2006). *Microfluidic diffusive filter for apheresis (leukapheresis)*. Lab Chip **6**, 83-9.

[118] Herzenberg LA, Parks D, et al. (2002). *The history and future of the fluorescence activated cell sorter and flow cytometry: a view from Stanford*. Clin Chem **48**, 1819-27.

[119] Zborowski M, Chalmers JJ (2011). *Rare Cell Separation and Analysis by Magnetic Sorting*. Anal Chem **83**, 8050–8056.

[120] Khademhosseini A, Yeh J, et al. (2005). *Cell docking inside microwells within reversibly sealed microfluidic channels for fabricating multiphenotype cell arrays*. Lab Chip **5**, 1380-6.

[121] Khademhosseini A, Ferreira L, et al. (2006). *Co-culture of human embryonic stem cells with murine embryonic fibroblasts on microwell-patterned substrates*. Biomaterials **27**, 5968-77.

[122] Park MC, Hur JY, et al. (2010). *High-throughput single-cell quantification using simple microwell-based cell docking and programmable time-course live-cell imaging*. Lab on a Chip DOI: 10.1039/C0LC00114G

[123] To LB, Haylock DN, et al. (1997). *The biology and clinical uses of blood stem cells*. Blood **89**, 2233-58.

[124] Jing Y, Moore LR, et al. (2007). *Negative selection of hematopoietic progenitor cells by continuous magnetophoresis*. Exp Hematol **35**, 662-72.

[125] Kreutz JE, Munson T, et al. (2011). *Theoretical design and analysis of multivolume digital assays with wide dynamic range validated experimentally with microfluidic digital PCR*. Anal Chem **83**, 8158-68.

[126] Desai TA, Tai YC, et al. (1997). *A MEMS Electrospray Nozzle for Mass Spectroscopy*. TRANSDUCERS '97, lnternational Conference on Solid-state Sensors and Actuators - Chicago, June 16-19, 1997, 927-930.

[127] Brown RB, Audet J (2008). *Current techniques for single-cell lysis*. J R Soc Interface **5 Suppl 2**, S131-8.